General Disclaimer

One or more of the Following Statements may affect this Document

- This document has been reproduced from the best copy furnished by the organizational source. It is being released in the interest of making available as much information as possible.

- This document may contain data, which exceeds the sheet parameters. It was furnished in this condition by the organizational source and is the best copy available.

- This document may contain tone-on-tone or color graphs, charts and/or pictures, which have been reproduced in black and white.

- This document is paginated as submitted by the original source.

- Portions of this document are not fully legible due to the historical nature of some of the material. However, it is the best reproduction available from the original submission.

TEST PROBLEMS FOR INVISCID TRANSONIC FLOW

AEROSPACE ENGINEERING DEPARTMENT

TEXAS A&M UNIVERSITY

LELAND A. CARLSON
PROFESSOR
AEROSPACE ENGINEERING DEPARTMENT
TEXAS A&M UNIVERSITY
COLLEGE STATION, TEXAS 77843

TEES REPORT NO. TAMRF-3224-7804

SEPTEMBER 1, 1979

TEXAS ENGINEERING EXPERIMENT STATION

TEST PROBLEMS FOR

INVISCID TRANSONIC FLOW

Leland A. Carlson
Professor
Aerospace Engineering Department
Texas A&M University
College Station, Texas 77843

TEES REPORT NO. TAMRF-3224-7804

September 1, 1979

PREFACE

This report constitutes a pre-presentation publication of a paper and results to be presented at the GAMM Workshop on "Numerical Methods for the Computation of Inviscid Transonic Flow with Shock Waves". This conference will be held at the Aeronautical Research Institute (FFA), Stockholm, Sweden on September 18-19, 1979.

This report includes the conference paper, all results obtained for the various workshop test cases, and approximate iso-mach line plots for the supercritical cases.

This work was primarily supported by NASA Grant NSG1174 and partially supported by the Texas Engineering Experiment Station.

TEST PROBLEMS FOR INVISCID TRANSONIC FLOW

Leland A. Carlson*
Texas A&M University
College Station, Texas, 77843

I. Introduction

This paper will briefly discuss some of the results obtained in the process of solving the test problems for the GAMM Workshop on "Numerical Methods for the Computation of Inviscid Transonic Flow with Shock Waves" with the TRANDES program. Briefly, this method,[1-5] utilizes the full, inviscid, perturbation-potential flow equation in a Cartesian grid system that is stretched to infinity. This equation is represented by a non-conservative system of finite difference equations that includes at supersonic points a rotated difference scheme and is solved by column relaxation. The solution usually starts from a zero perturbation potential on a very coarse grid (typically 13 x 7) followed by several grid halvings until a final solution is obtained on a fine grid (97x49). Occasionally, for cases having high local Mach numbers, the solution must be started on the coarse grid (25 x 13). Since the airfoil does not coincide with the grid points, the surface boundary conditions are represented as two-term Taylor series about dummy points inside the airfoil. On the outer boundaries, the exact infinity conditions are used. This method can, if desired, include the effects of weak viscous interaction or be used in the design mode. [2-6]

All of the results presented at the workshop and in this paper were obtained at the rate of 10^4 pts/sec on an Amdahl 470/V6 using a FORTG compiler and single precision arithmetic (less than 7 significant digits). A typical run took 4-8 minutes, although good engineering results were obtained in one minute on the medium grid; and convergence was obtained on the medium grid to at least a maximum cyclic perturbation change of less than 5E-5. On the fine grid, the $\Delta\phi$max was usually larger due to significant digit error in the far-field. It should be noted that the workshop cases were run 1.5-5.0 times longer than usual due to the availability of computer time from TAMU, and that the TRANDES program has never been optimized for time.

In order to maintain the goal of common discretization, the grid stretchings were setup so that the number of airfoil points, number of wake points, Δx and Δy at the trailing edge, and the location of the last finite vertical grid column matched the suggested grids as closely as possible. For cases involving large supersonic zones, the y-grid was extended so that the last finite horizontal grid line was subsonic. Otherwise, the rotated difference scheme might have used undefined values.

* Professor, Aerospace Engineering Department

for the test cases appear to show correct trends. (I.E. For $C_L = 0.0$ --$M_\infty = 0.72$, CD = .0004; $M_\infty = 0.8$, CD = 0.0100; M = 0.85, CD = 0.0381; $M_\infty = 0.95$, CD = 0.0989)

b. Bump in Channel

This problem was solved by treating the bump as a symmetrical airfoil in a solid wall wind-tunnel. The solution used 41 points on the upper surface, 16 in the wake, 21 pts vertically from the centerline to the wall, $\Delta X_{te} = 0.0251$, $\Delta Y_{te} = 0.03$, and $\phi_y = 0$ on the channel walls. For the upstream/downstream infinity conditions two approaches were tried. The first used the asymptotic form derived by Murman[8] while the second had $\phi_x = 0$ imposed and allowed the solution to float. The results on the bump and between it and the wall were identical. However, some slight differences were observed upstream and downstream, with the floating solution showing less blockage type influence. While the floating approach is easier to implement, it is more prone to significant digit errors due to the magnitude of the floating potential (O(1) instead of O(0.1)).

Finally, several other upstream/downstream boundary conditions were imposed, such as ϕ=0; and all yielded essentially the same results. Since the channel case was coded rapidly for the workshop, this lack of sensitivity may be due to either coding errors or a special feature of the test case.

c. RAE 2822

This problem was solved using the same grid as for the NACA 0012 cases. During the solutions, it was discovered that the subcritical results were sensitive to the location of the first and last points on the airfoil, which are normally at 0.01c and 0.99c (X4 = 0.49). The initial results (solid line, Fig. 2) indicated a possible peak in C_{pu} near the leading edge. To resolve this peak, the first points were moved to 0.005c and 0.995c (X4 = 0.495), and slightly different results were obtained as shown on Fig. 2. Interestingly, EPSS had to be increased to 1.0 for this second case due to the appearance of supersonic points on the coarser grinds. Obviously, the Cartesian grid placement sometimes affects the airfoil effective α; and it is probably best to correlate results versus C_L rather than α.

d. CAST 7

Again the basic NACA 0012 grid was used. Here, in both the subcritical and supercritical cases, oscillations were observed in C_{pl} at 0.03c and in C_{pu} at 0.92c. Since the surface slopes were also oscillatory in these areas, it is believed this behavior was due to the sparsity of the given coordinates and the use of spline fits to determine the computational ordinates and slopes. Also, in both cases, the

aft C_{pl} bucket turned around at the TE and approached stagnation. This behavior is reasonable due to the large TE angle (12.5°). In actuality, viscous effects would mitigate this trend.

e. KORN 1

The basic NACA 0012 grid was also used for this case. For the design point, the resultant C_p distribution was close to the theoretical hodograph values and was almost shockless. Again some sensitivity to the grid size and X4 value was observed, as can be seen in Fig. 3. Also, a double precision calculation (16 digits) was made and essentially yielded the same results as with single precision (7 digits). However, for the 16 digit case the $\Delta\phi$max on the fine grid was steadily decreasing instead of oscillatory and smaller (6E-5 vs. 2E-4).

III. Conclusions

Except for the NACA 0012, M_∞ = 0.95 case, all test problems were solved straight-forwardly and appeared to be converged or close to convergence. The only difficulty was some sensitivity to grid placement, which is typical of the Cartesian formulation. Again, note that all results were obtained in single precision (less than 7 significant digits) on an Amdahl 470/V6.

IV. Acknowledgments

This work was primarily supported by NASA Grant NSG 1174 and partially supported by the Texas Engineering Experiment Station. The author expresses his appreciation to Robert Simmons, TAMU Aerospace Engineering Department, for his assistance in the preparation of the figures.

V. References

1. Carlson, L.A., "Transonic Airfoil Analysis and Design Using Cartesian Coordinates," J. of Arcft, Vol. 13, May 1976 pp. 349-356.
2. Carlson, L.A., "Transonic Airfoil Flowfield Analysis Using Cartesian Coordinates," NASA CR-2577, Aug. 1975.
3. Carlson, L.A., "TRANDES: A Fortran Program for Transonic Airfoil Analysis and Design," NASA CR-2821, June 1977.
4. Carlson, L.A., "Inverse Transonic Airfoil Design Including Viscous Interaction," NASA CP-2001, Nov. 1976, pp 1387-1395.
5. Carlson, L.A. and Rocholl, B.M., "Application of Direct Inverse Techniques to Airfoil Analysis and Design," NASA CP-2045, Pt. 1, pp 55-72.
6. Carlson, L.A., "Test Problems for Inviscid Transonic Flow," Texas Engr. Expt. Station Rept. TAMRF-3224-7904, 1979.
7. Lock, R.C., "Test Cases for Numerical Methods in Two Dimensional Transonic Flow," AGARD Rept R-575-70, 1970.
8. Murman, E.M., "Computation of Wall Effects on Ventilated Transonic Wind Tunnels," AIAA Paper No. 72-1007, Sept. 1972.

Summary of Test Problem Results

Problem	Airfoil	M_∞	α	CL	CD	CMC4	EPSS	Comments
A-I (i)	NACA 0012	0.72	0.0°	0.0	0.0004	0.0	----	
(ii)	"	0.63	2.0°	0.339	-0.0002	-0.002	----	
II(i)	"	0.80	0.0°	0.0	0.0100	0.0	0.4	
(ii)	"	0.85	0.0°	0.0	0.0381	0.0	0.6	
(iii)	"	0.95	0.0°	0.0	0.0958	0.0	1.0	
(iv)	"	0.80	1.25°	0.321	0.0199	-0.035	0.6	
(v)	"	0.85	1.00°	0.283	0.0444	-0.075	0.8	
B	Bump	0.85	0.0°	0.0	0.0240	0.0	0.6	Murman Asymptotic
	"	"	"	0.0	0.0236	0.0	0.4	Floater
C-I	RAE 2822	0.676	1.0°	0.551	0.0047	-0.106	0.4	X4 = 0.49
	"	"	"	0.574	-0.0043	-0.109	1.0	X4 = 0.495
II	"	0.75	3.0°	1.154	0.0583	-0.210	0.8	
D-I	CAST 7	0.70	-1.0°	0.436	0.0065	-0.138	----	
II	"	0.76	0.5°	0.898	0.0259	-0.210	0.8	
G-I	KORN 1	0.75	0.115°	0.622	0.0012	-0.160	0.4	X4 = .4925, Single Precision
	"	"	"	0.609	0.0074	-0.148	0.4	X4 = .49, FFA Grid
	"	"	"	0.606	0.0058	-0.147	0.4	X4 = .49, St'd Grid
	"	"	"	0.624	0.0012	-0.150	0.4	X4 = .4925, Double Precision
G-II	"	"	1.0°	0.833	0.0181	-0.171	0.6	

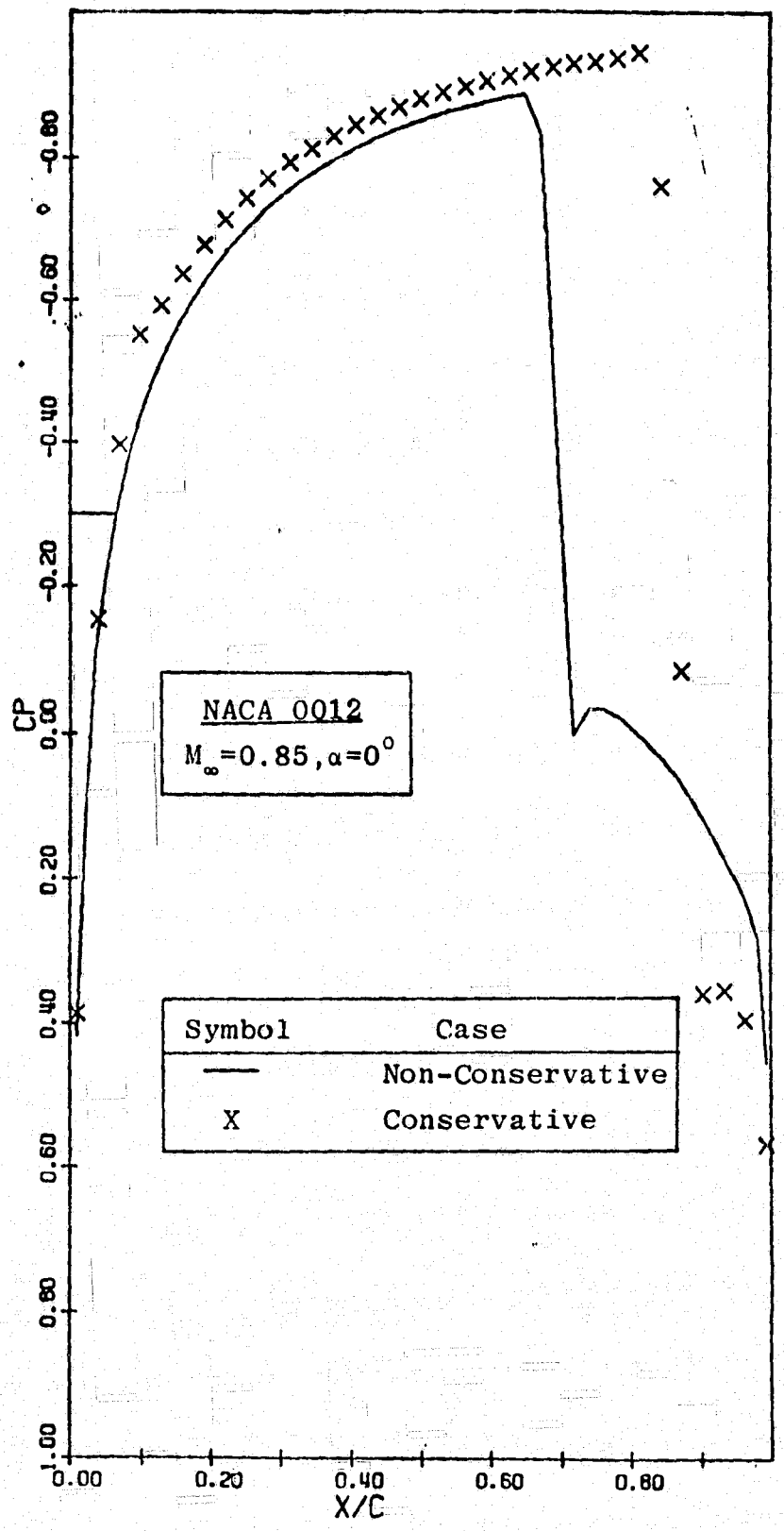

Figure 1: Non-Conservative versus Conservative Results

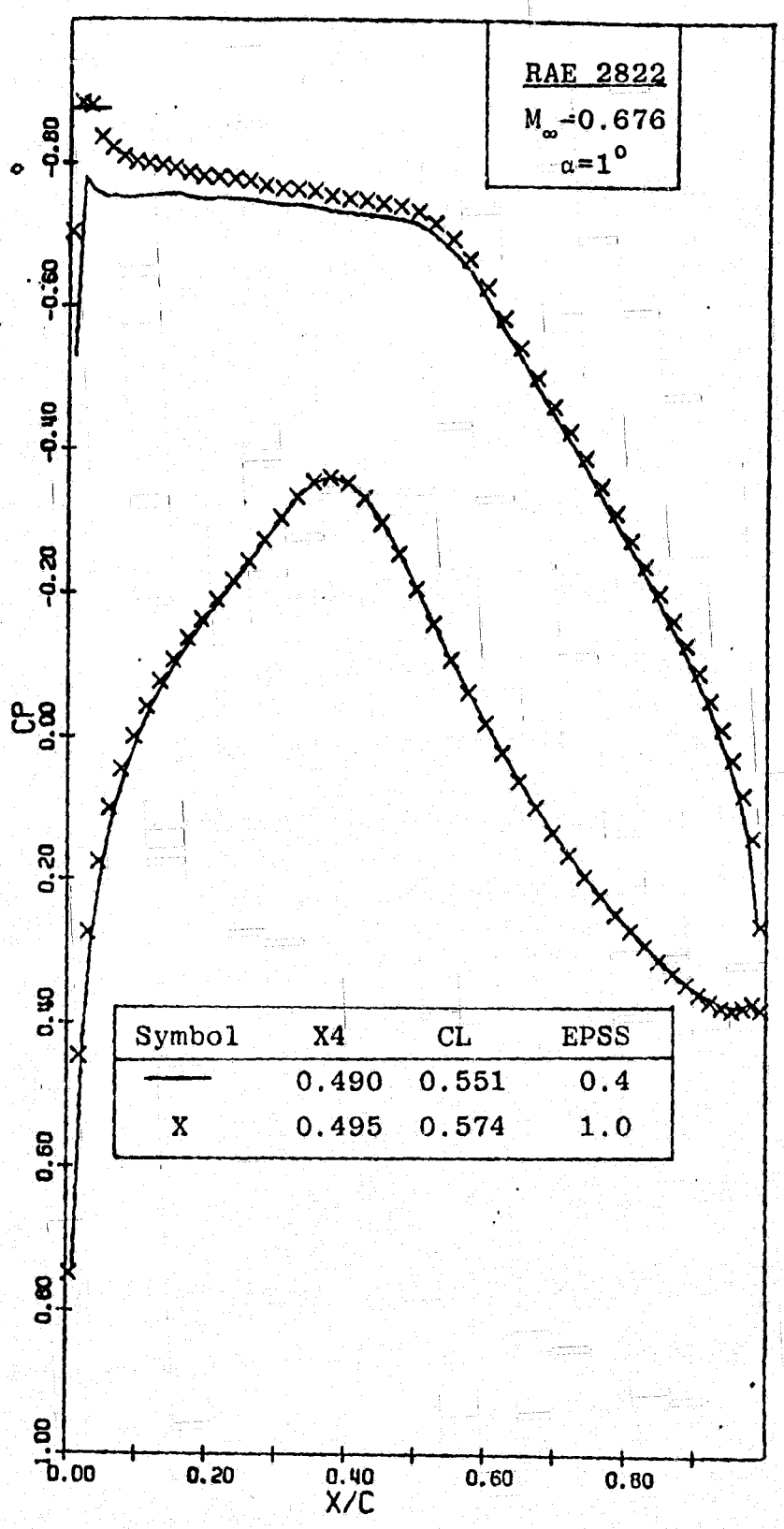

Figure 2: The Effect of Grid Placement on C_p

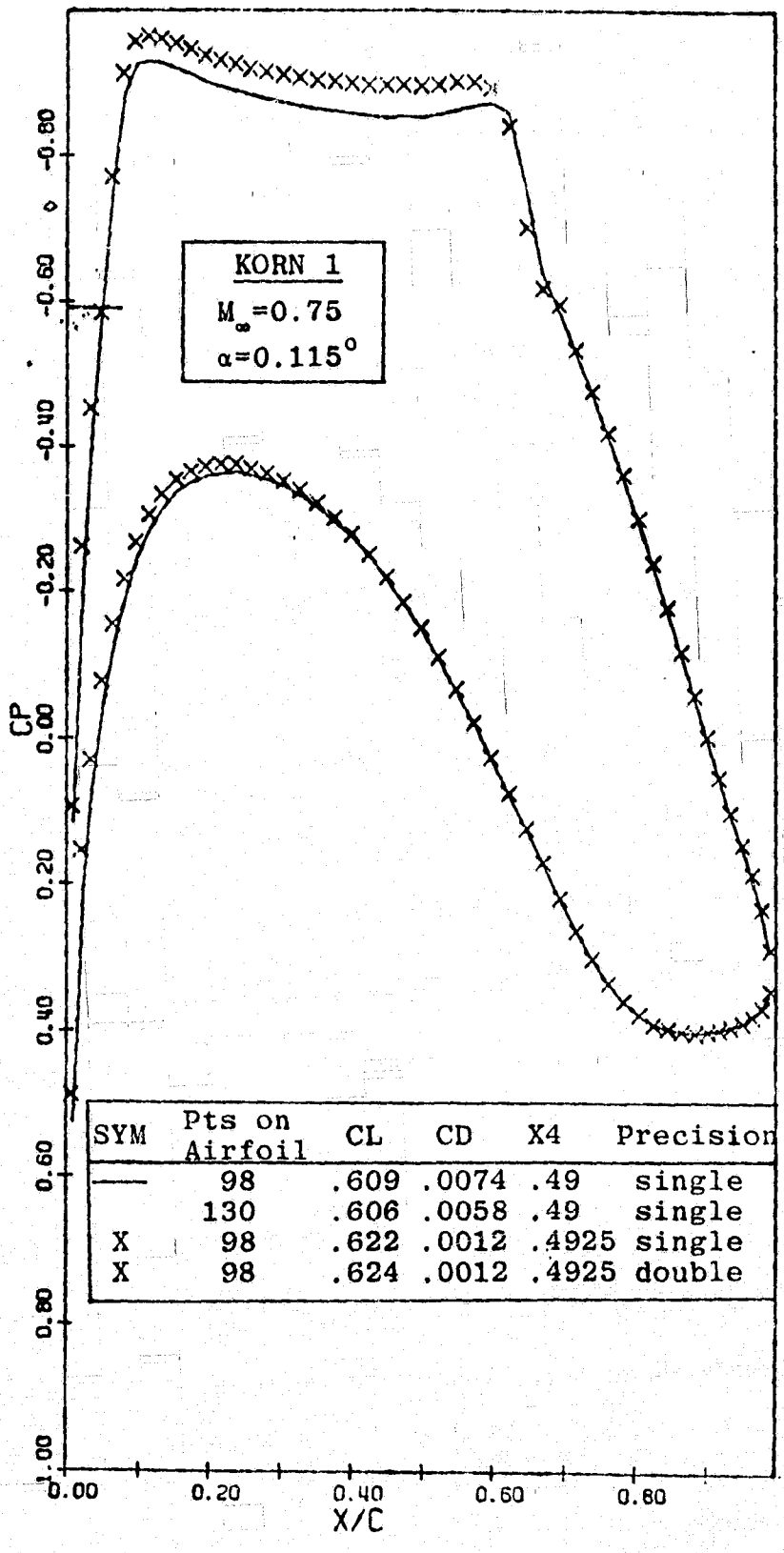

Figure 3: Results for the KORN 1 Airfoil

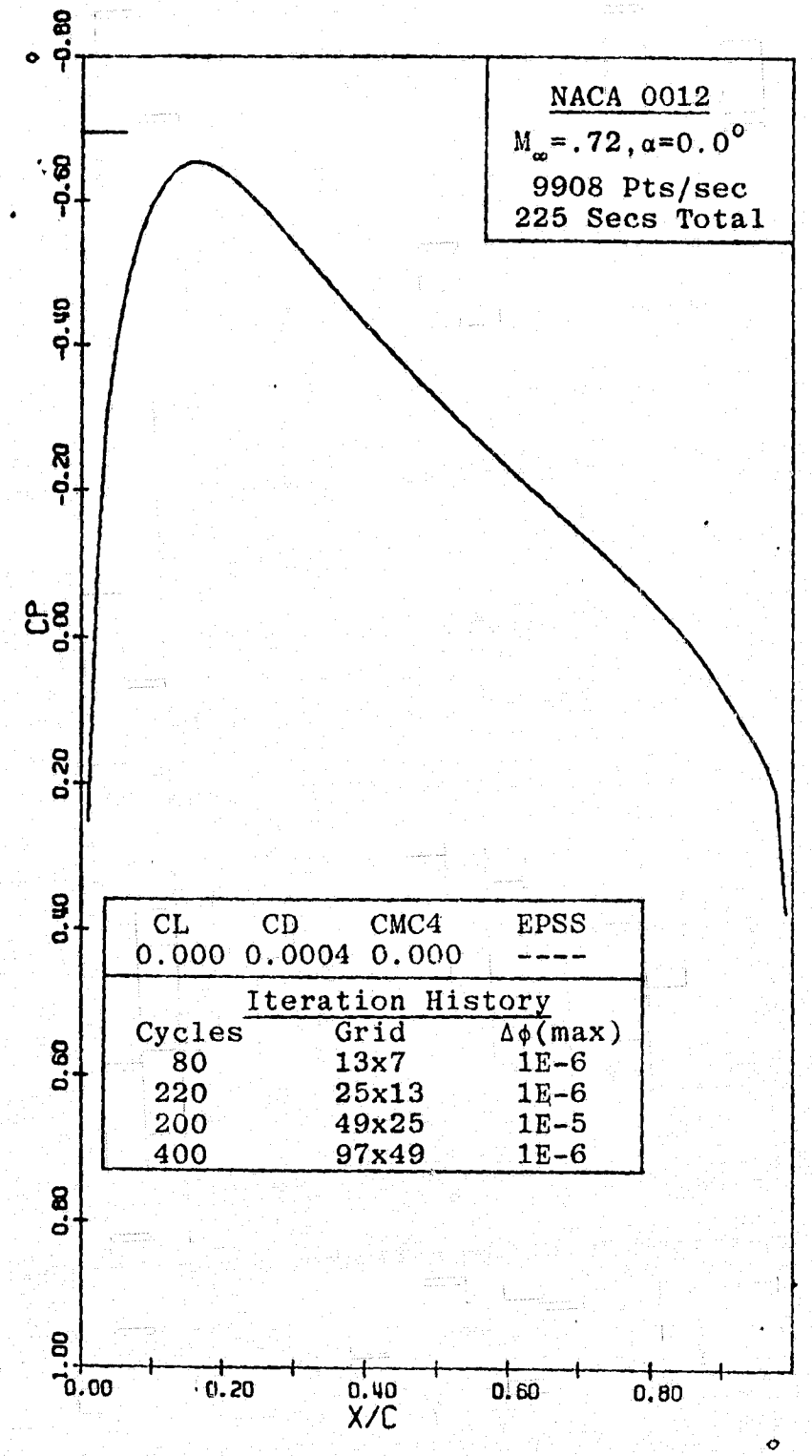

Figure 1: Case A-I(i), Airfoil C_p Distribution versus X/C

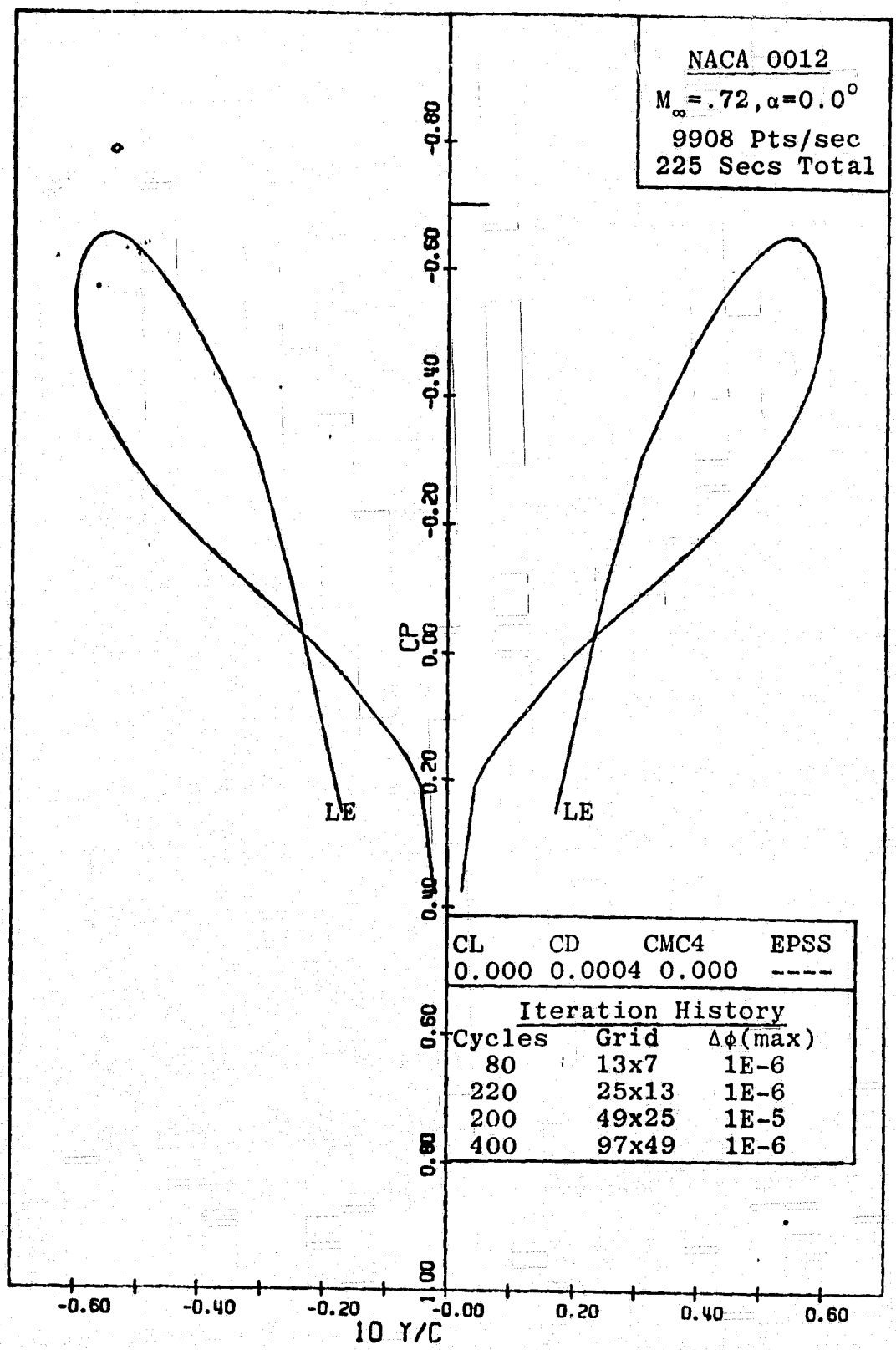

Figure 2: Case A-I(i), Airfoil C_p Distribution versus Y/C

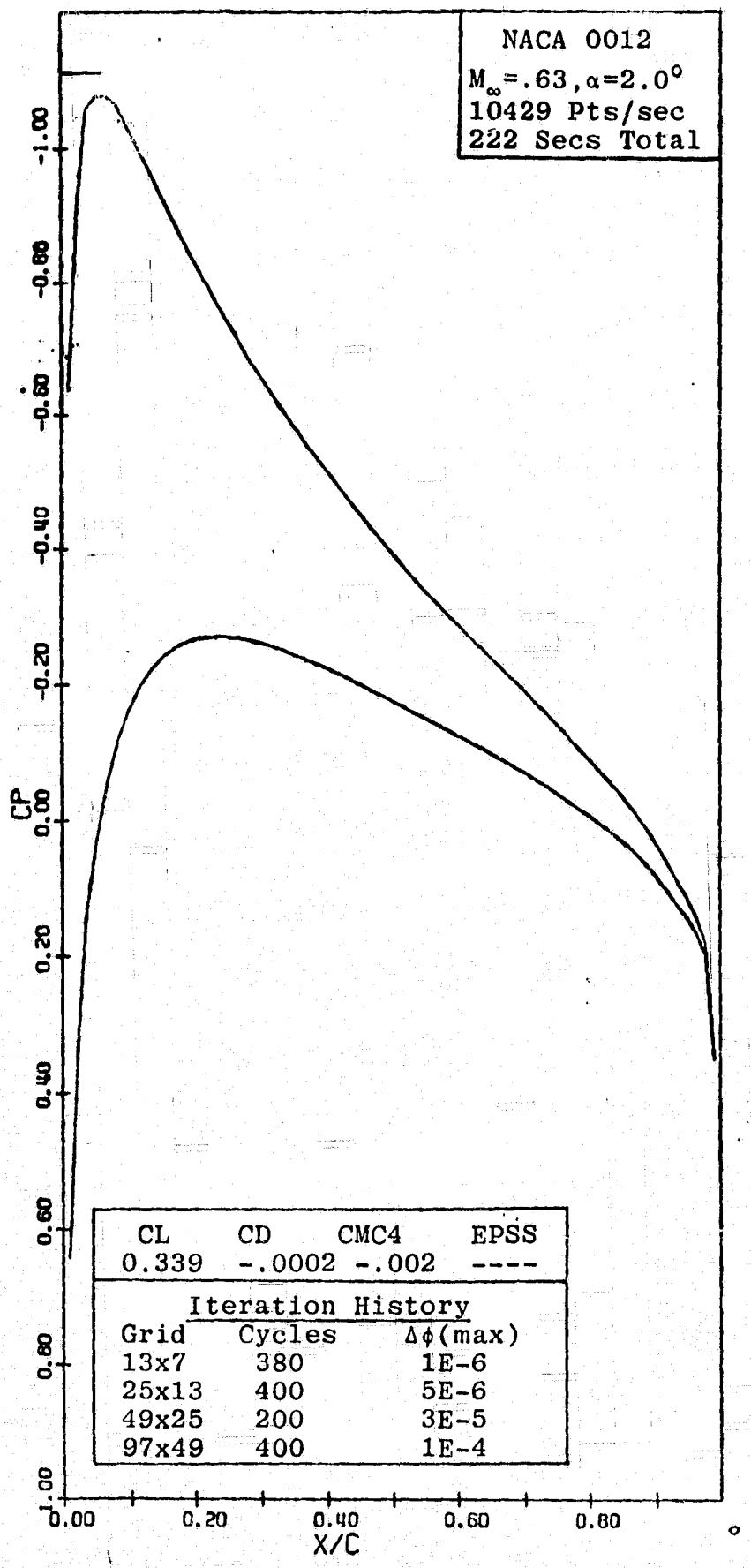

Figure 3: Case A-I(ii), Airfoil C_p Distribution versus X/C

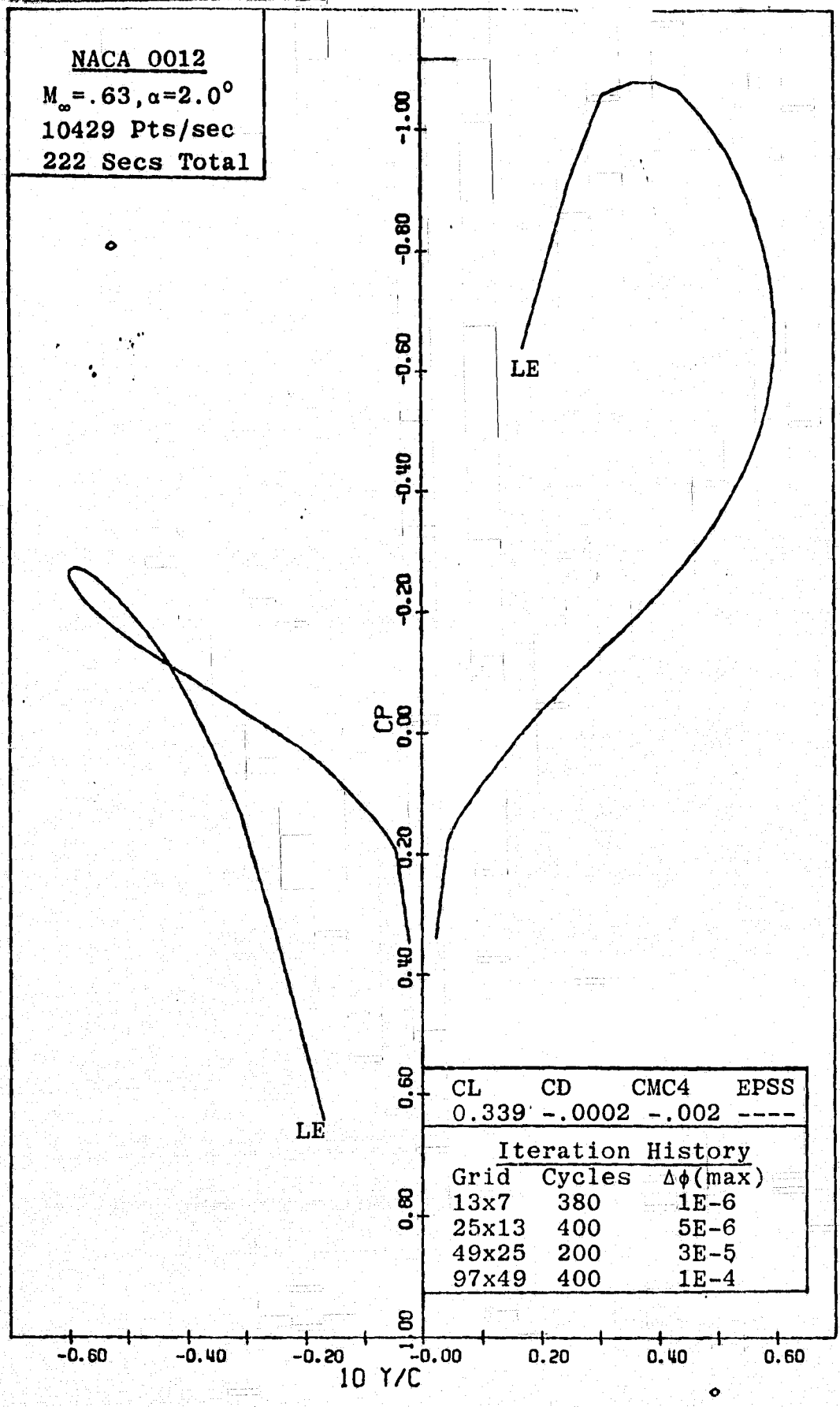

Figure 4: Case A-I(ii), Airfoil C_p Distribution versus Y/C

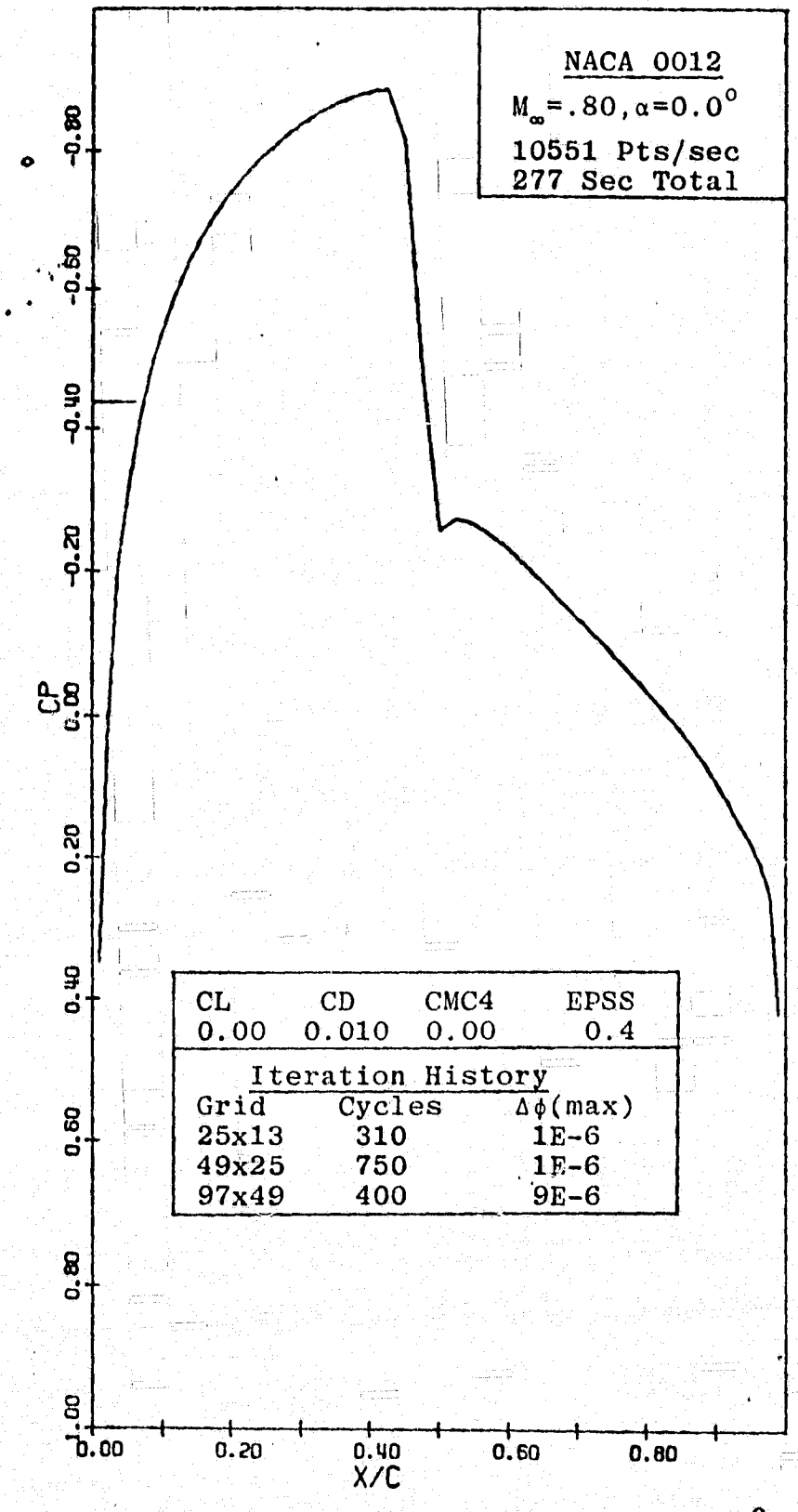

Figure 5: Case A-II(i), Airfoil C_p Distribution versus X/C

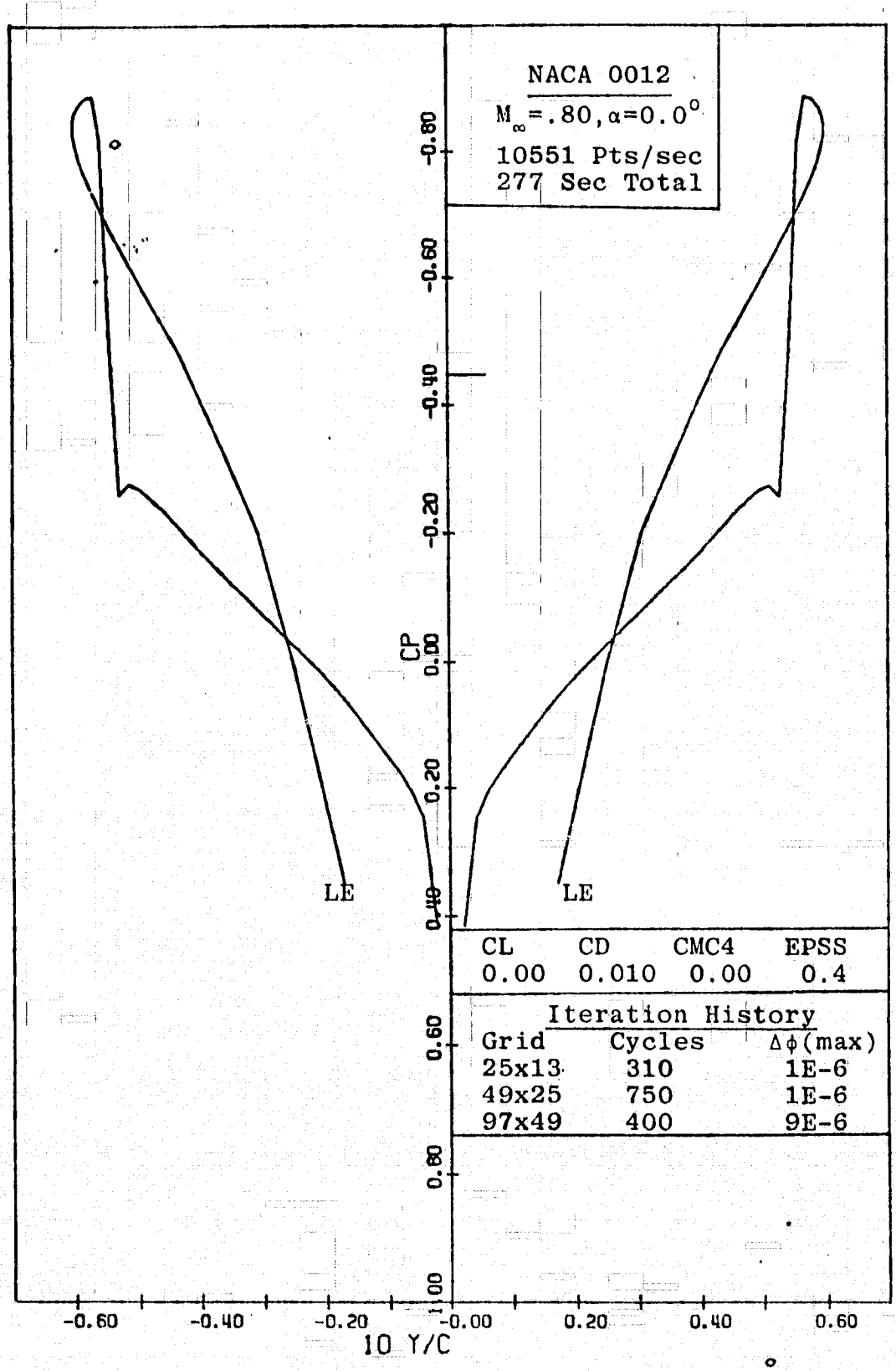

Figure 6: Case A-II(i), Airfoil C_p Distribution versus Y/C

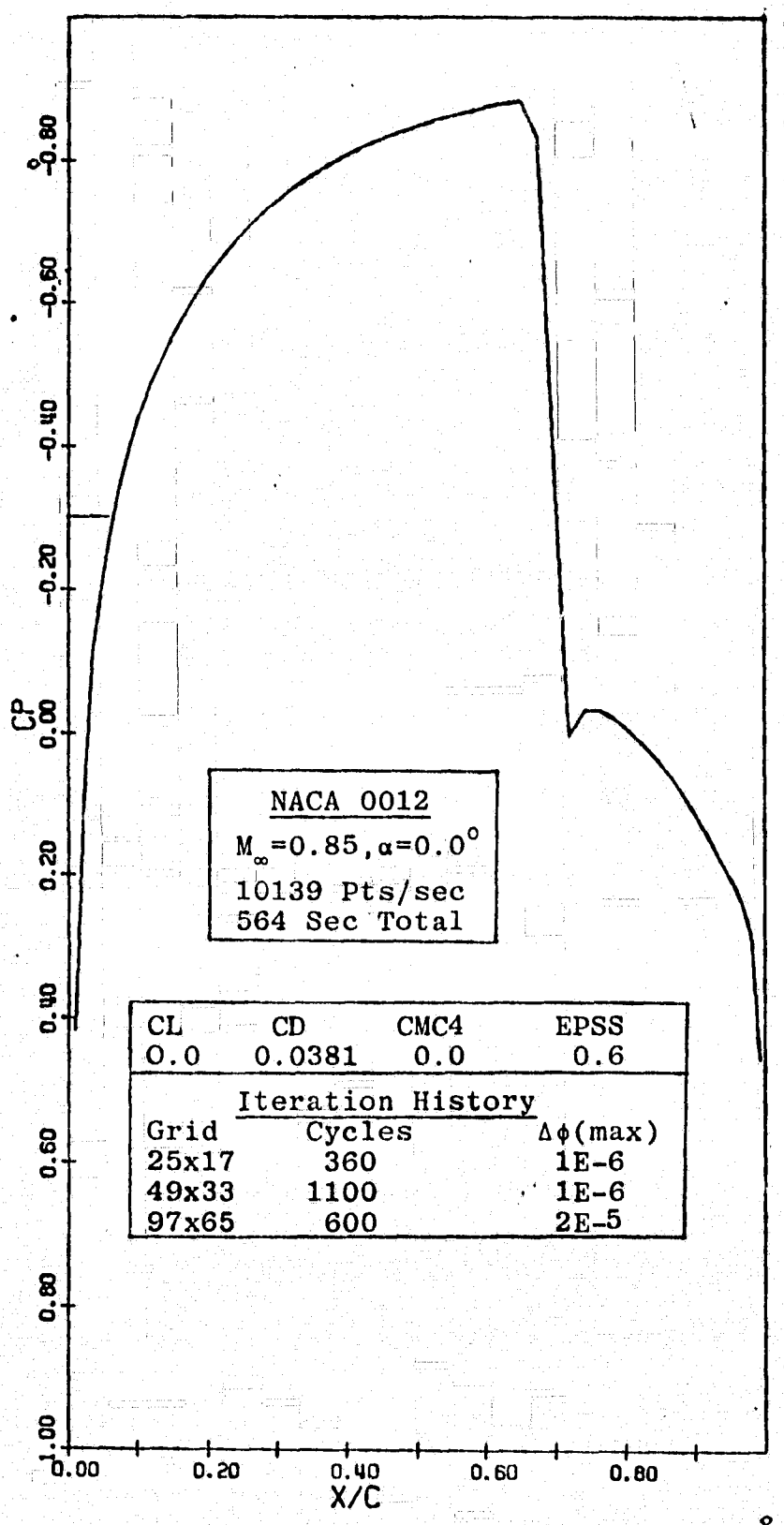

Figure 7: Case A-II(ii), Airfoil C_p Distribution versus X/C

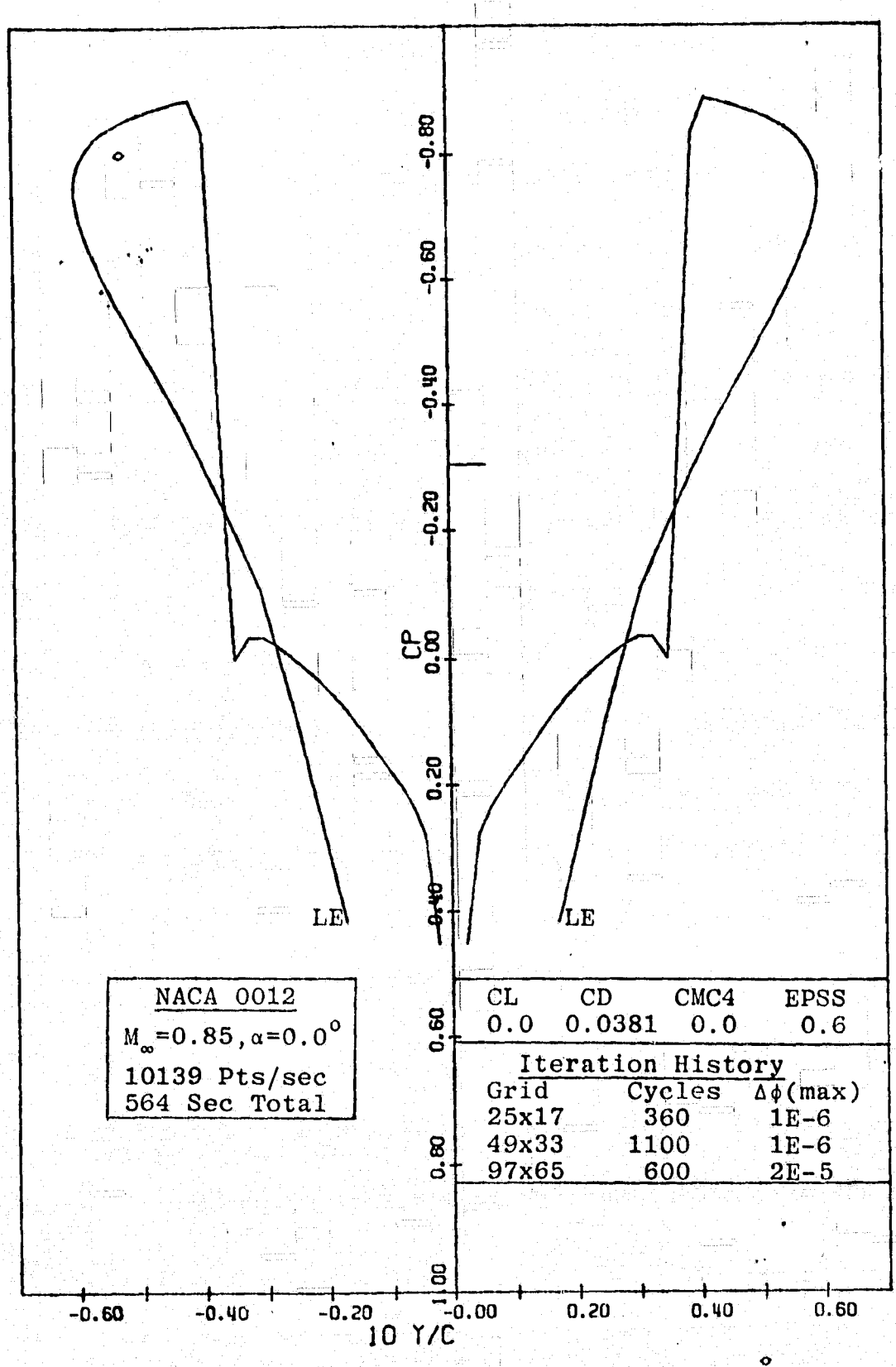

Figure 8: Case A-II(ii), Airfiol C_p Distribution versus Y/C

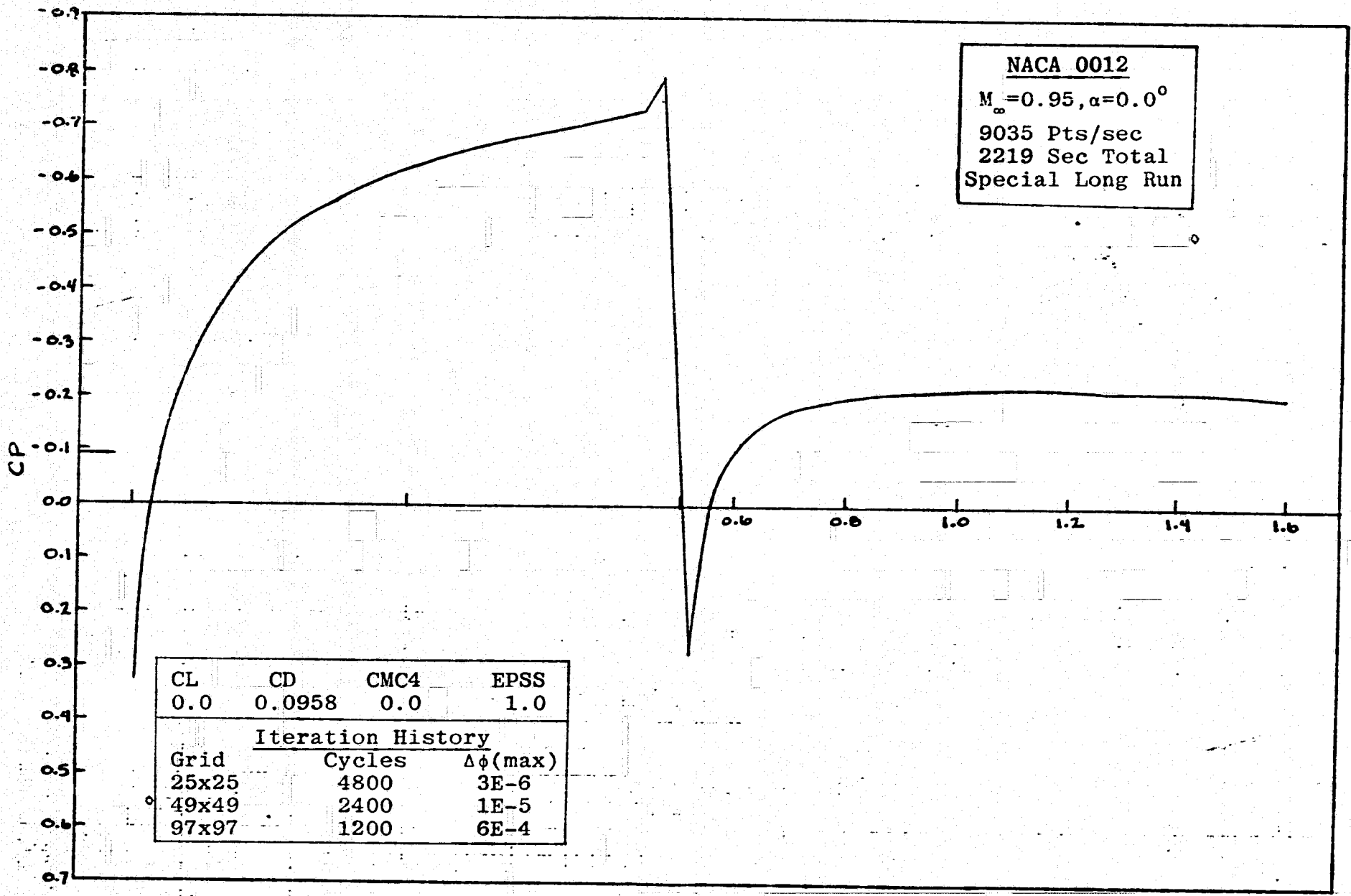

Figure 9: Case A-II(iii), Airfoil C_p Distribution versus X/C

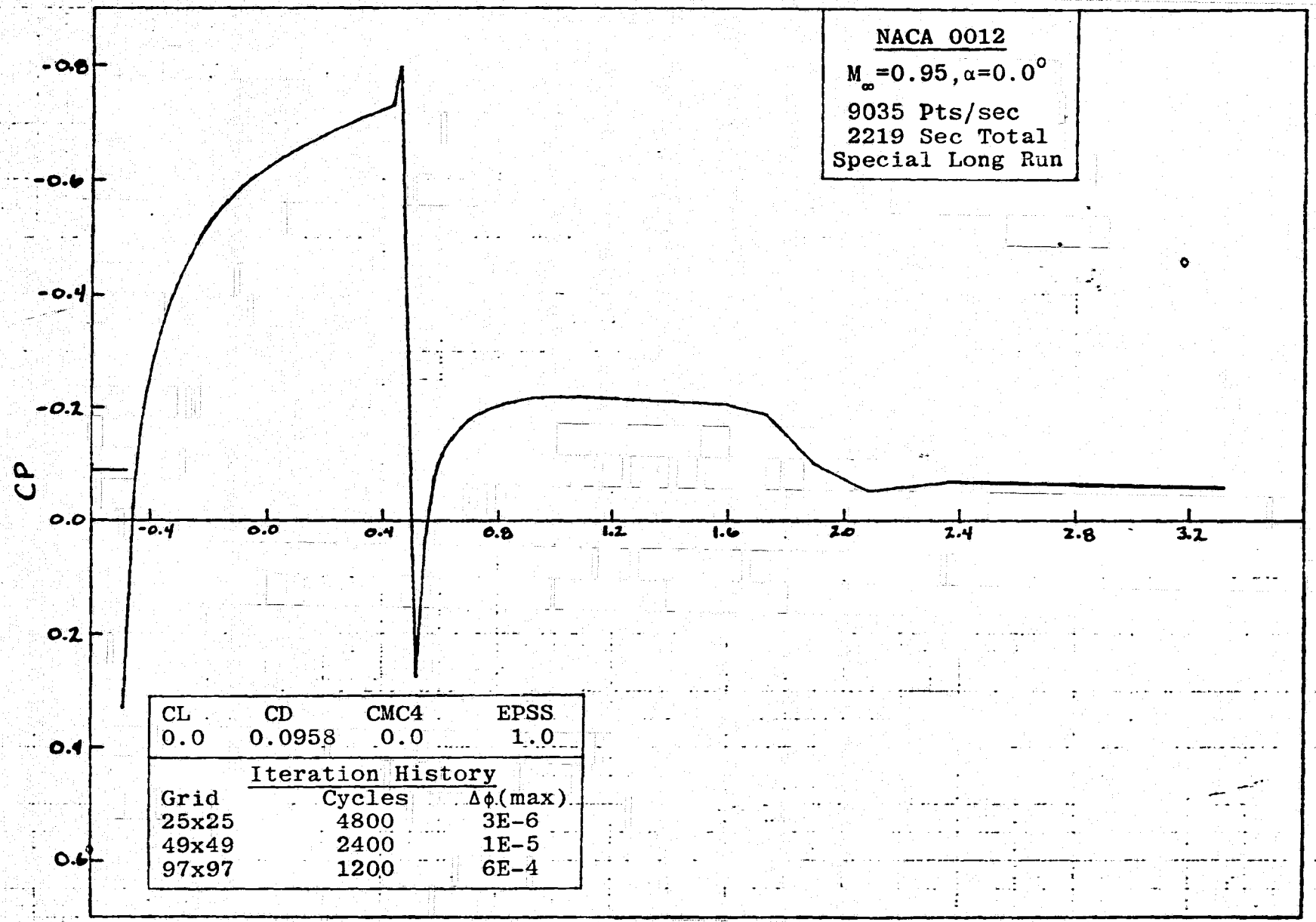

Figure 10: Case A-II(iii), Airfoil C_p Distribution versus X/C, into wake region

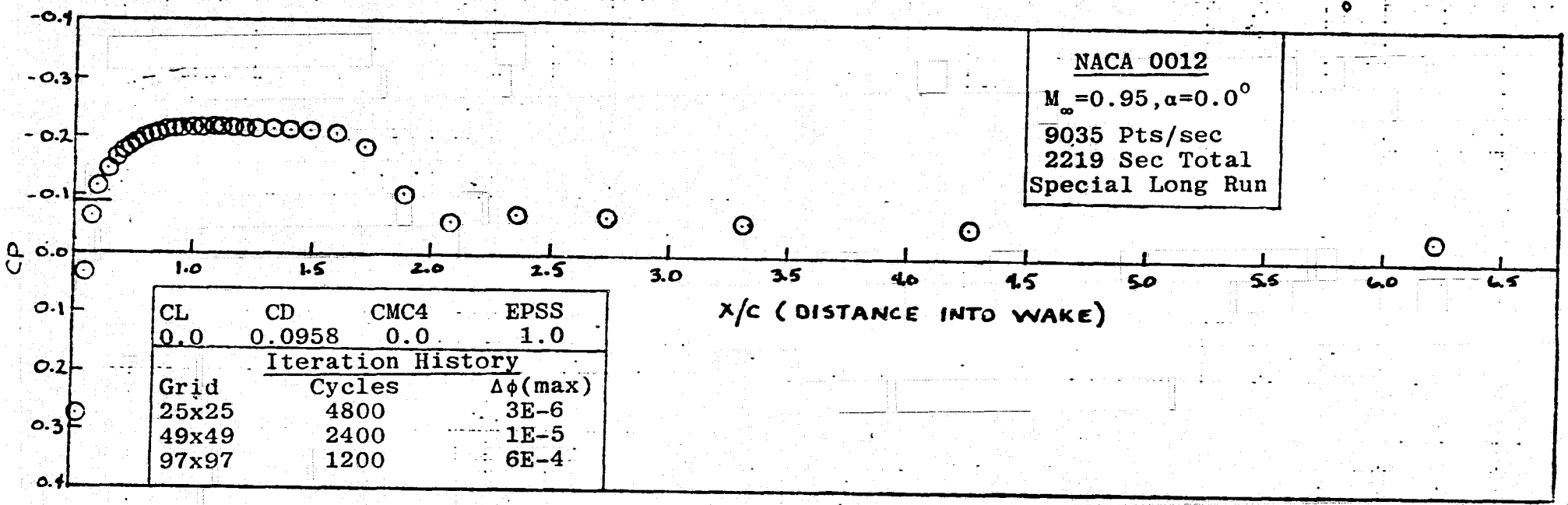

Figure 11: Case A-II(iii), Wake C_p Distribution versus X/C

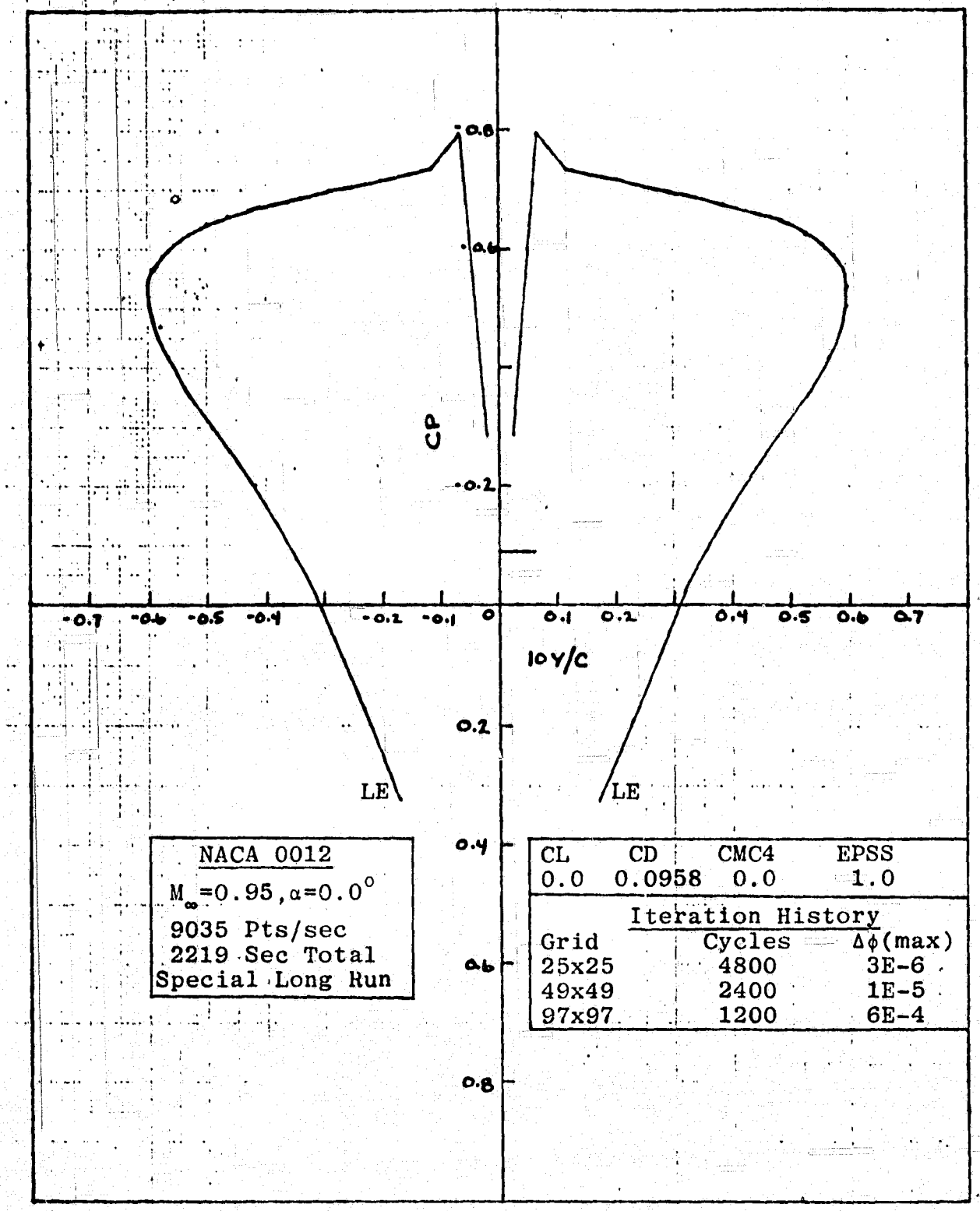

Figure 12: Case A-II(iii), Airfoil C_p Distribution versus Y/C

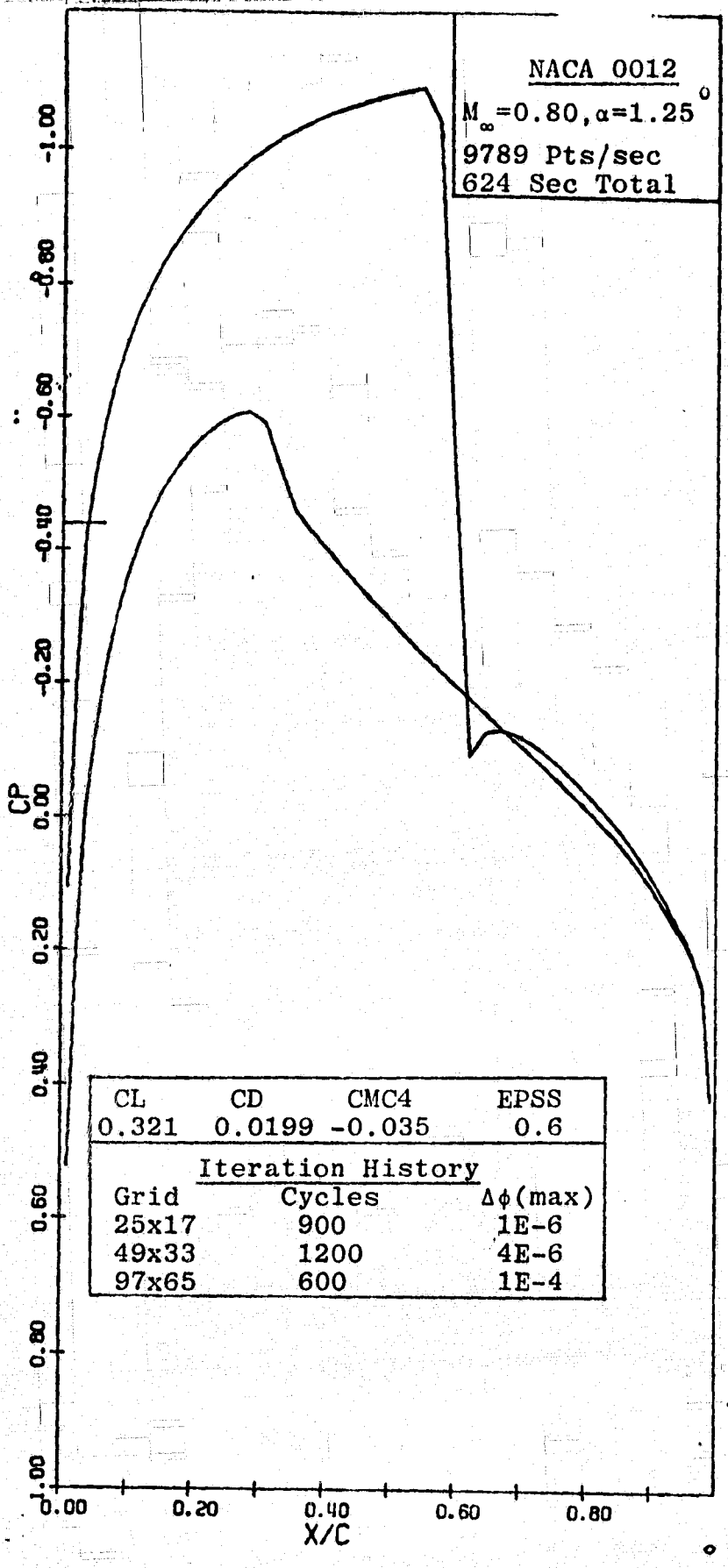

Figure 13: Case A-II(iv), Airfoil C_p Distribution versus X/C

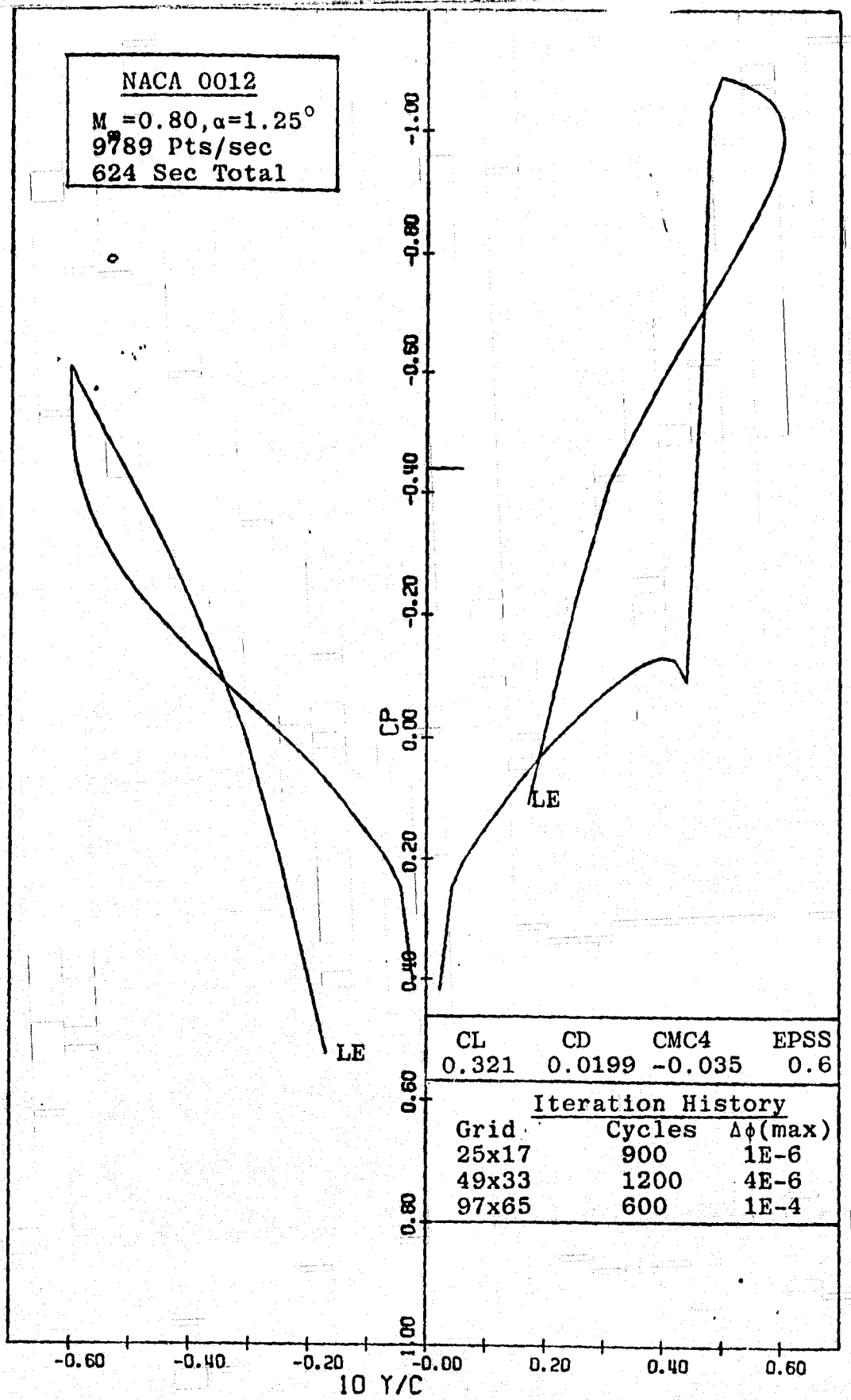

Figure 14: Case A-II(iv), Airfoil C_p Distribution versus Y/C

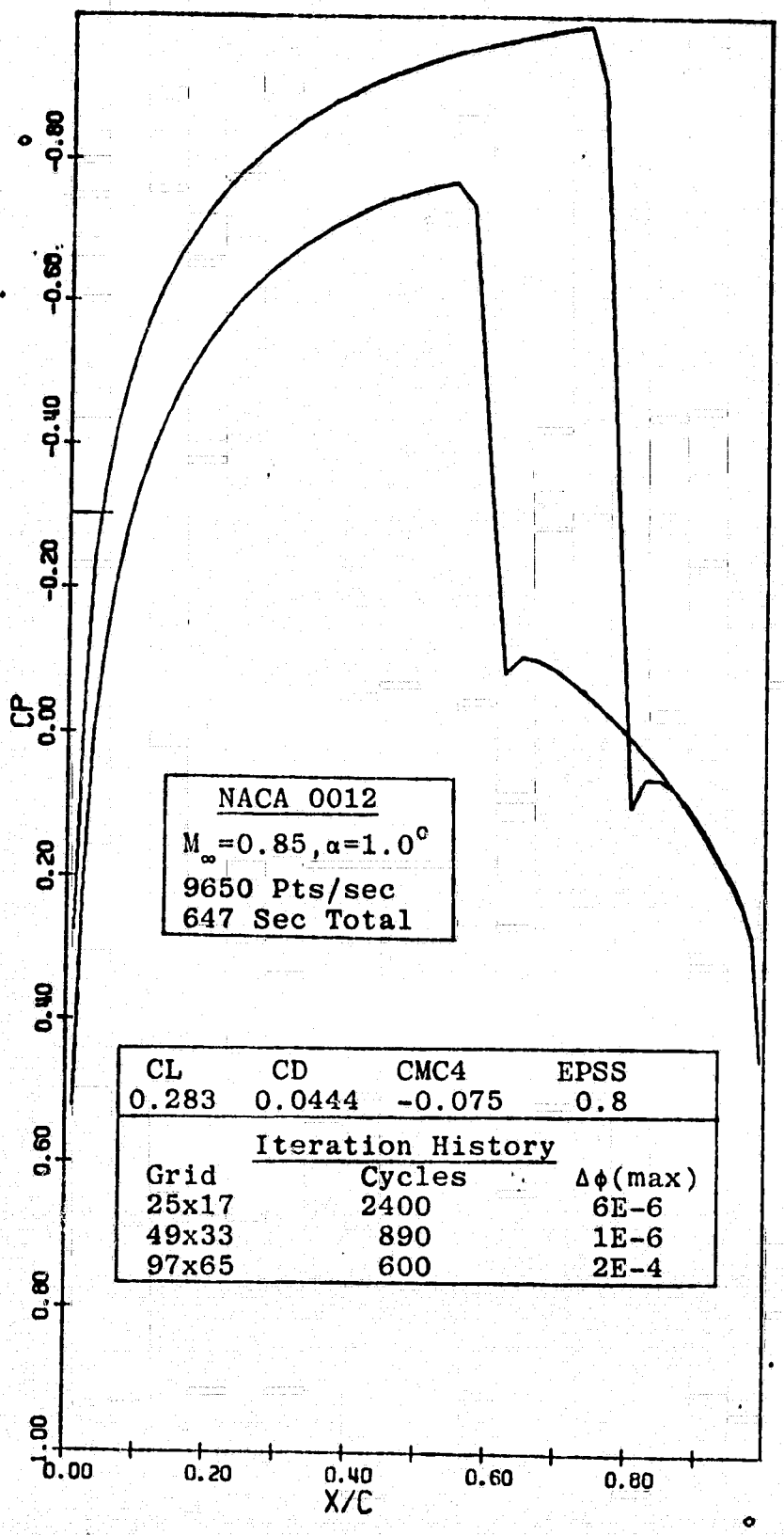

Figure 15: Case A-II(v), Airfoil C_p Distribution versus X/C

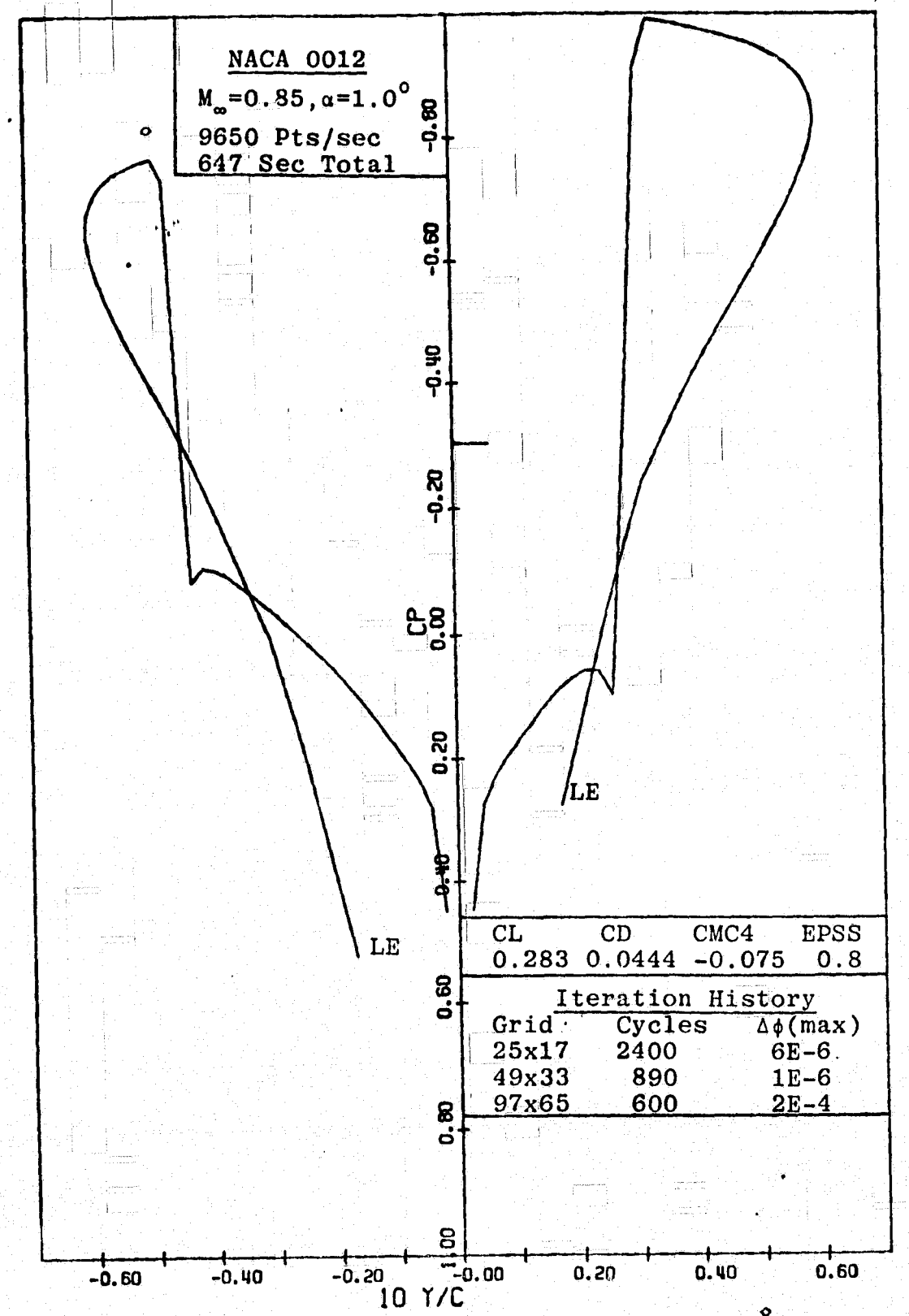

Figure 16: Case A-II(v), Airfoil C_p distribution versus Y/C

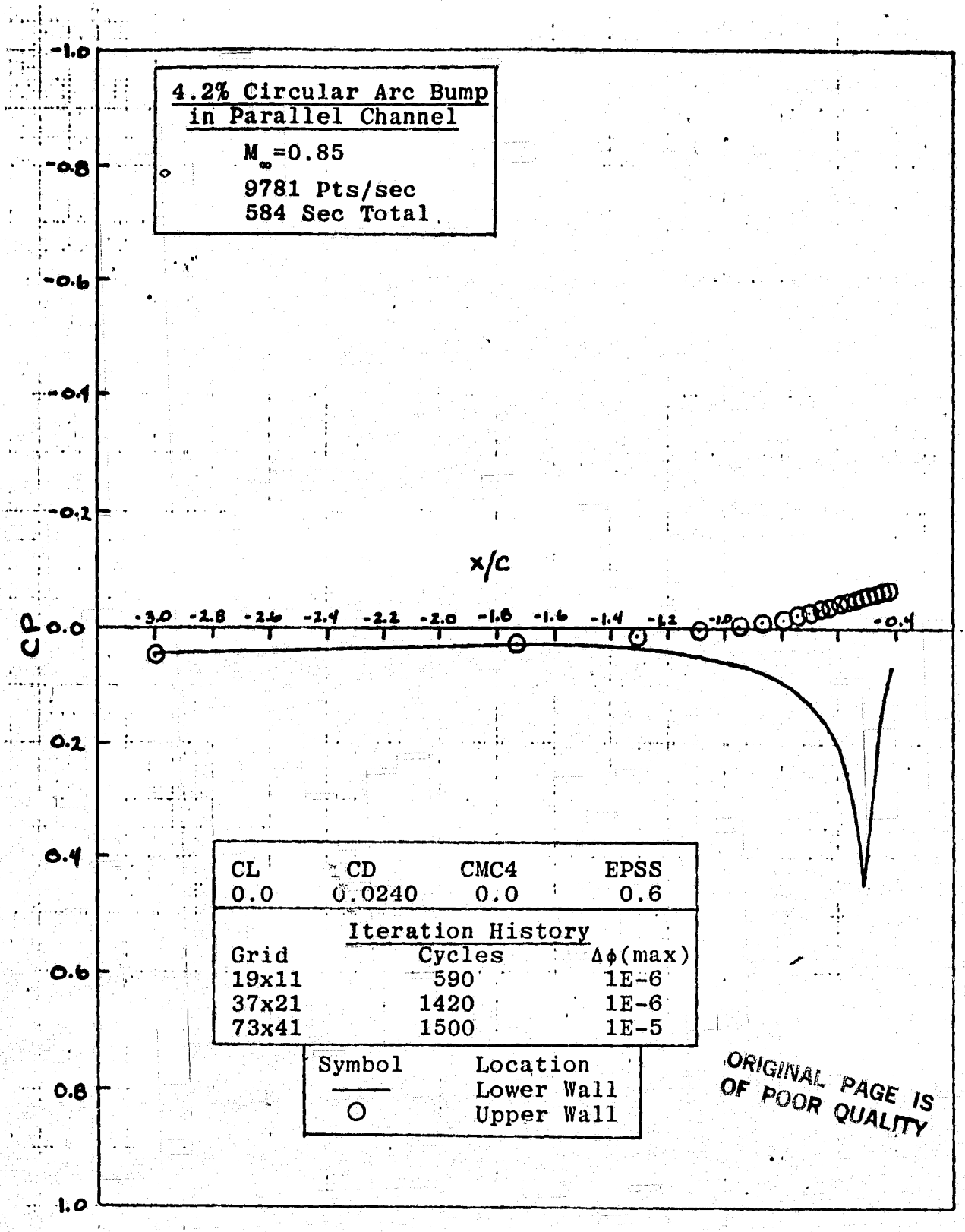

Figure 17: Case B, Upstream C_p Distribution

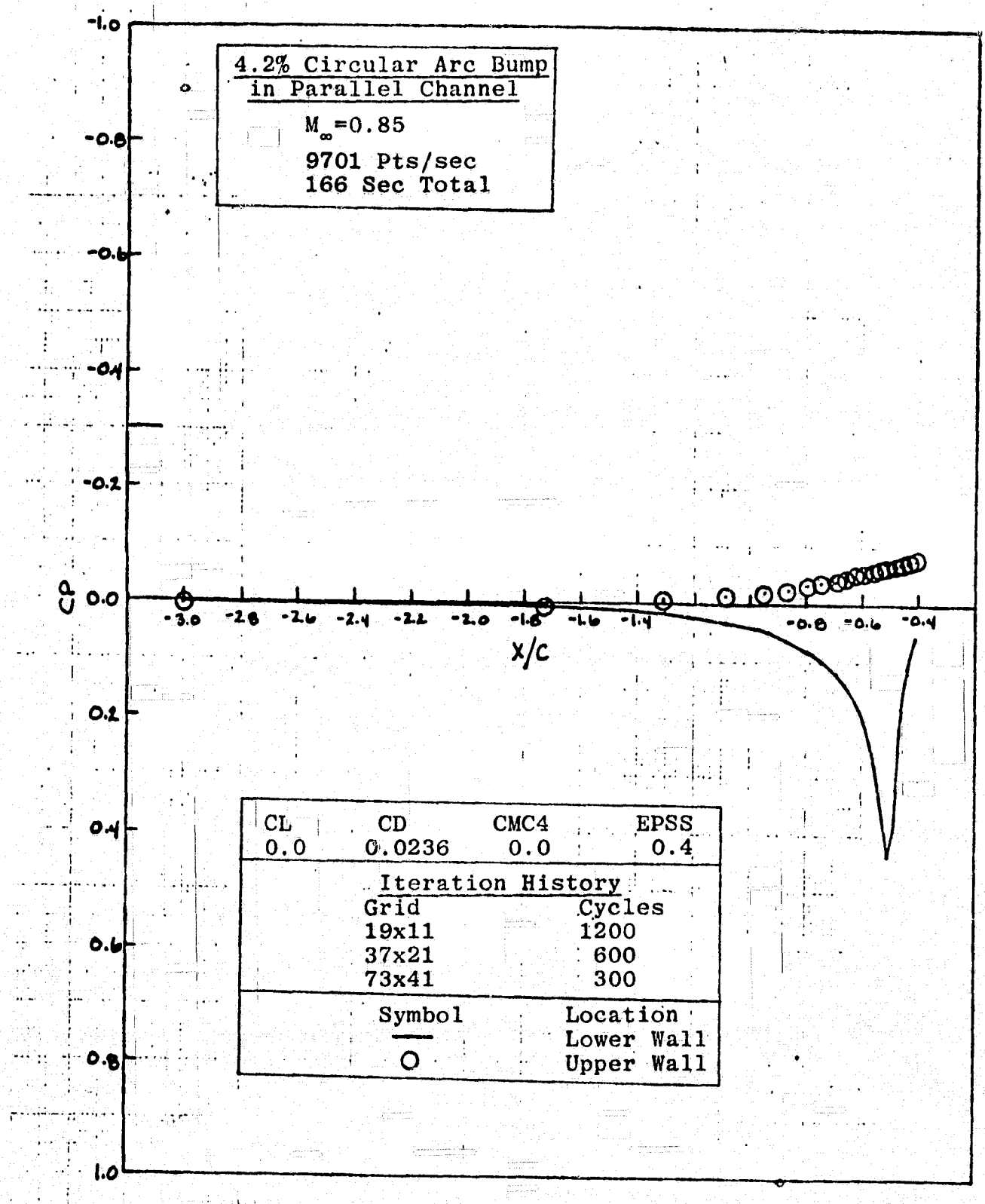

Figure 17a: Case B, Upstream C_p Distribution, Floater Solution

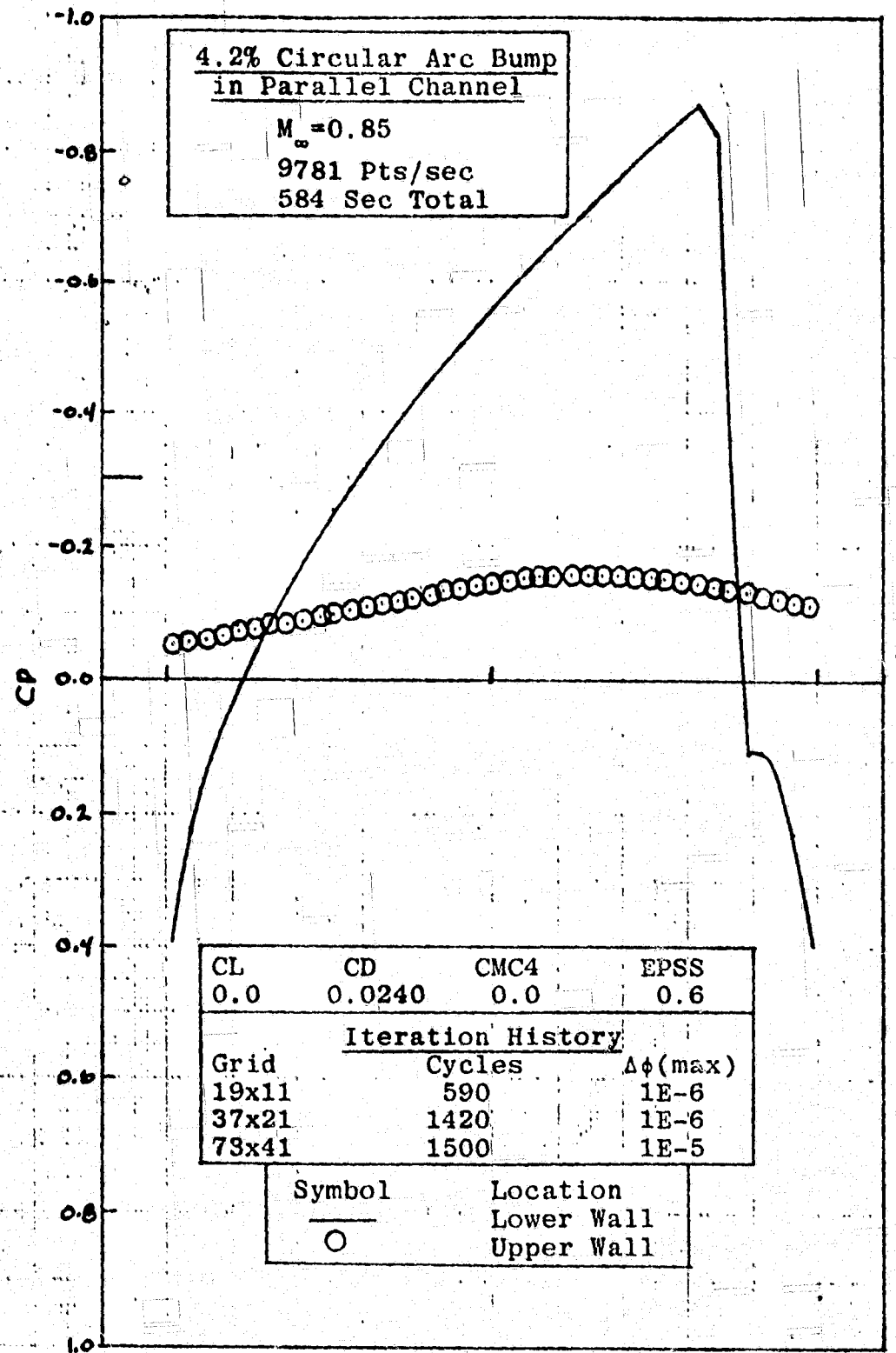

Figure 18: Case B,"Bump" C_p Distribution versus X/C_o

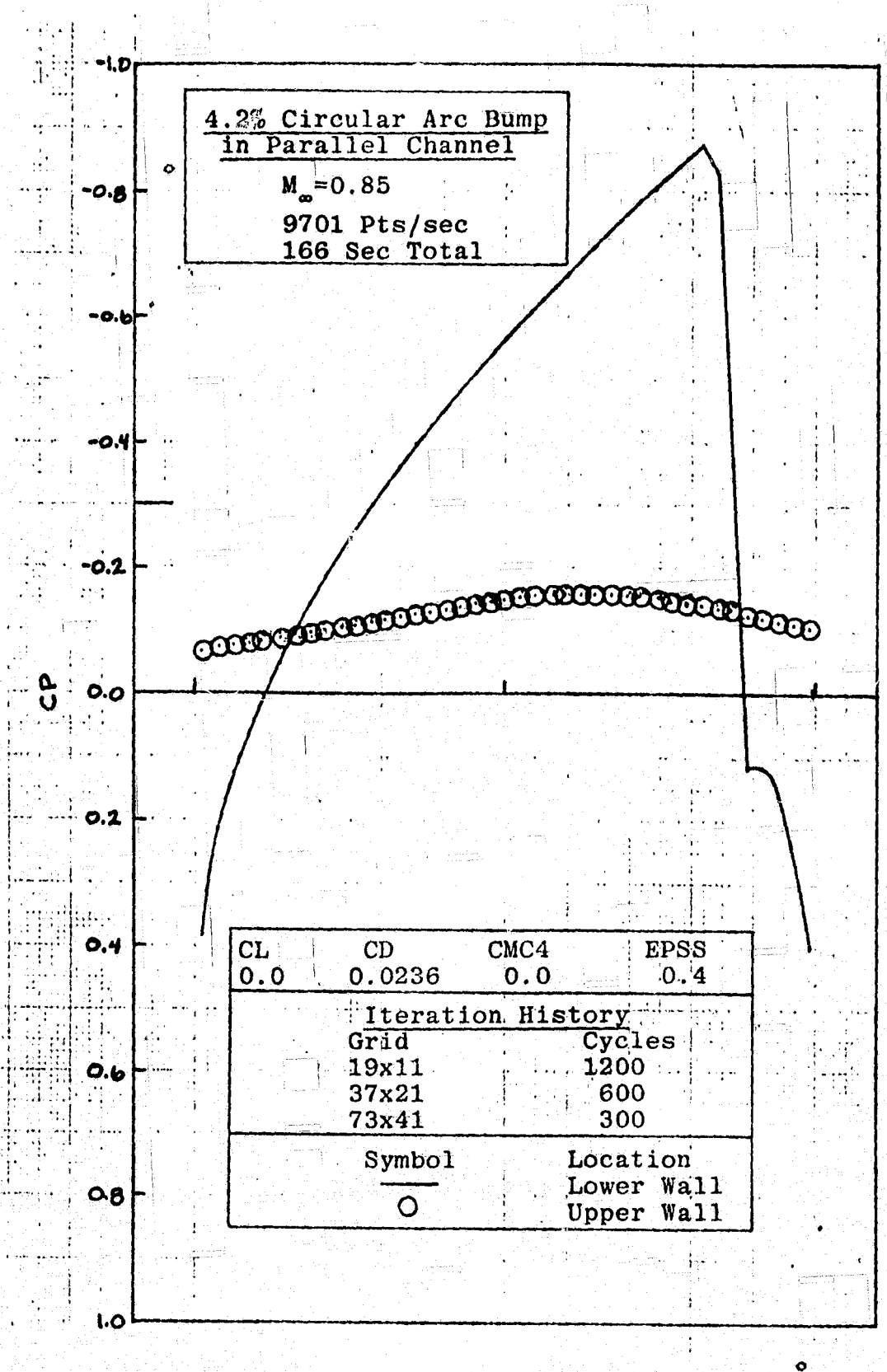

Figure 18a: Case B,"Bump" C_p Distribution versus X/C, Floater Solution

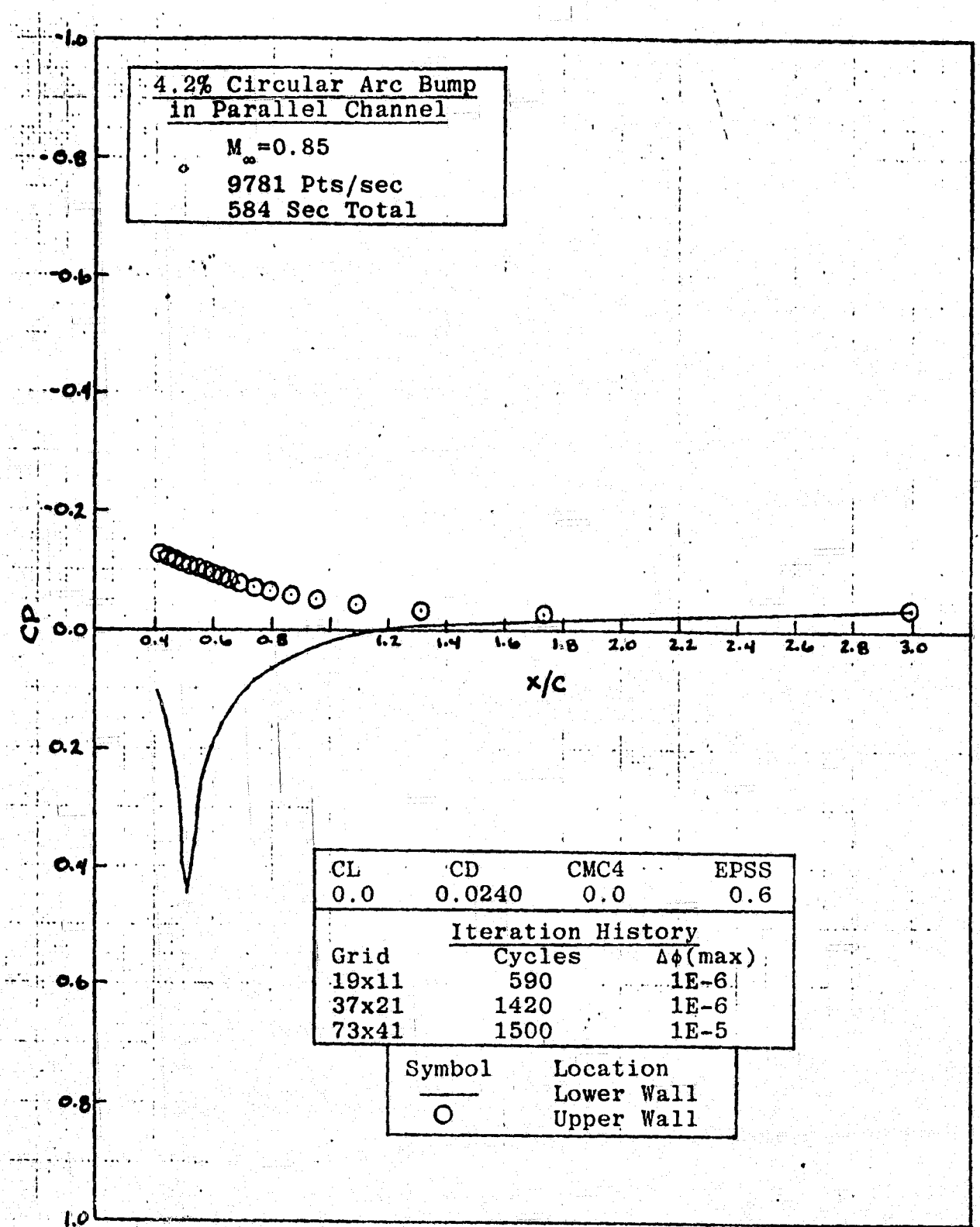

Figure 19: Case B, Downstream C_p Distribution

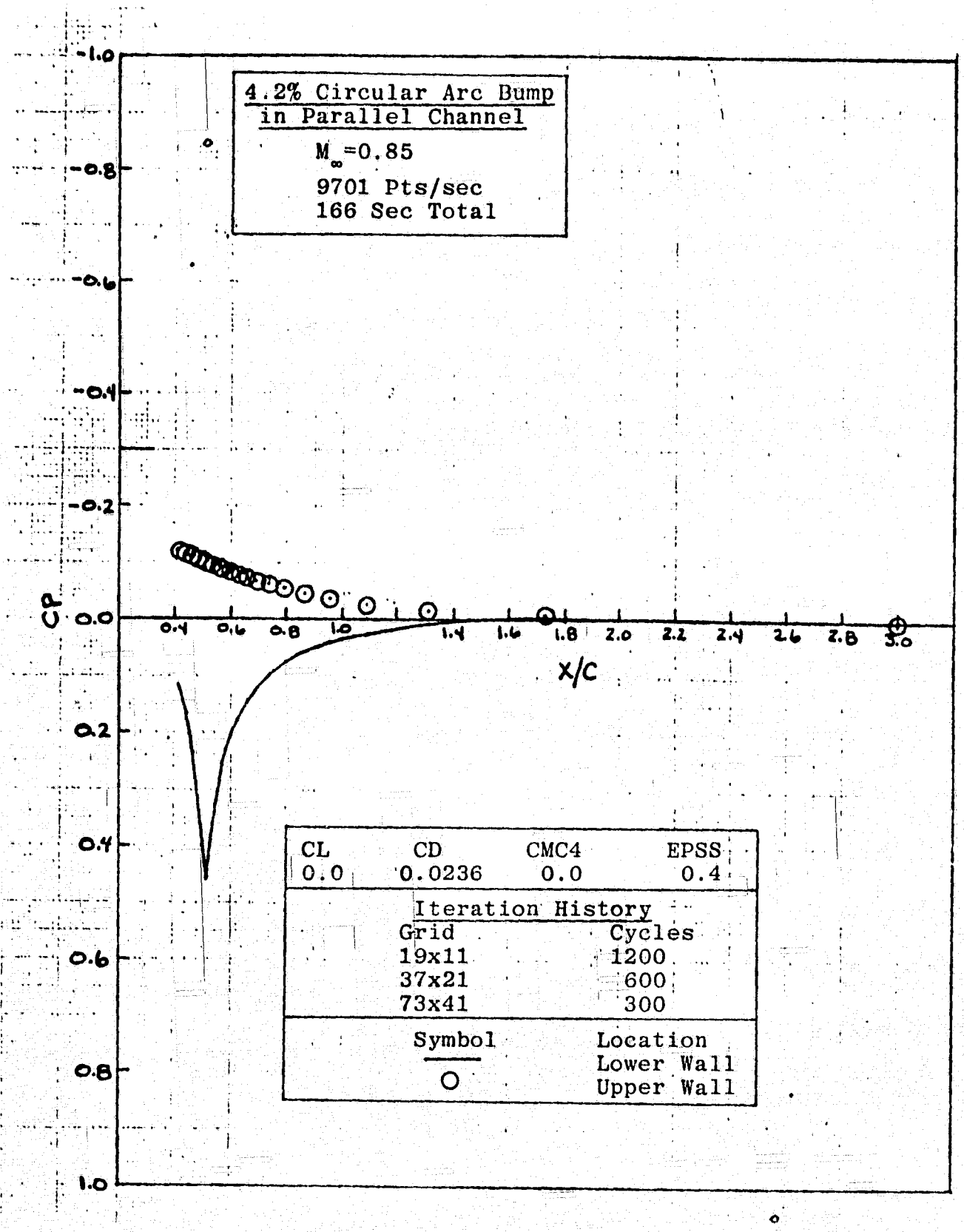

Figure 19a: Case B, Downstream C_p Distribution, Floater Solution

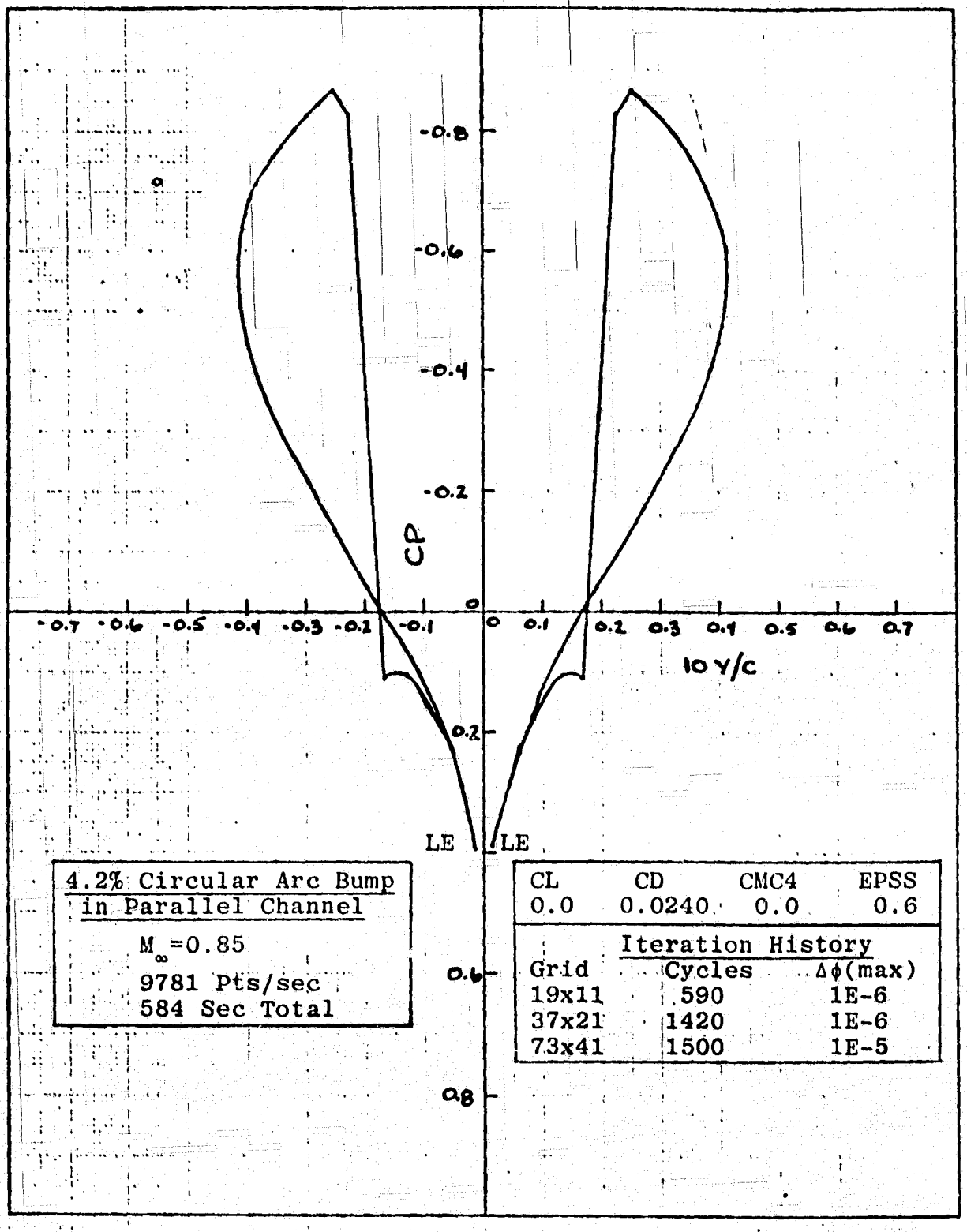

Figure 20: Case B,"Bump" C_p Distribution versus Y/C

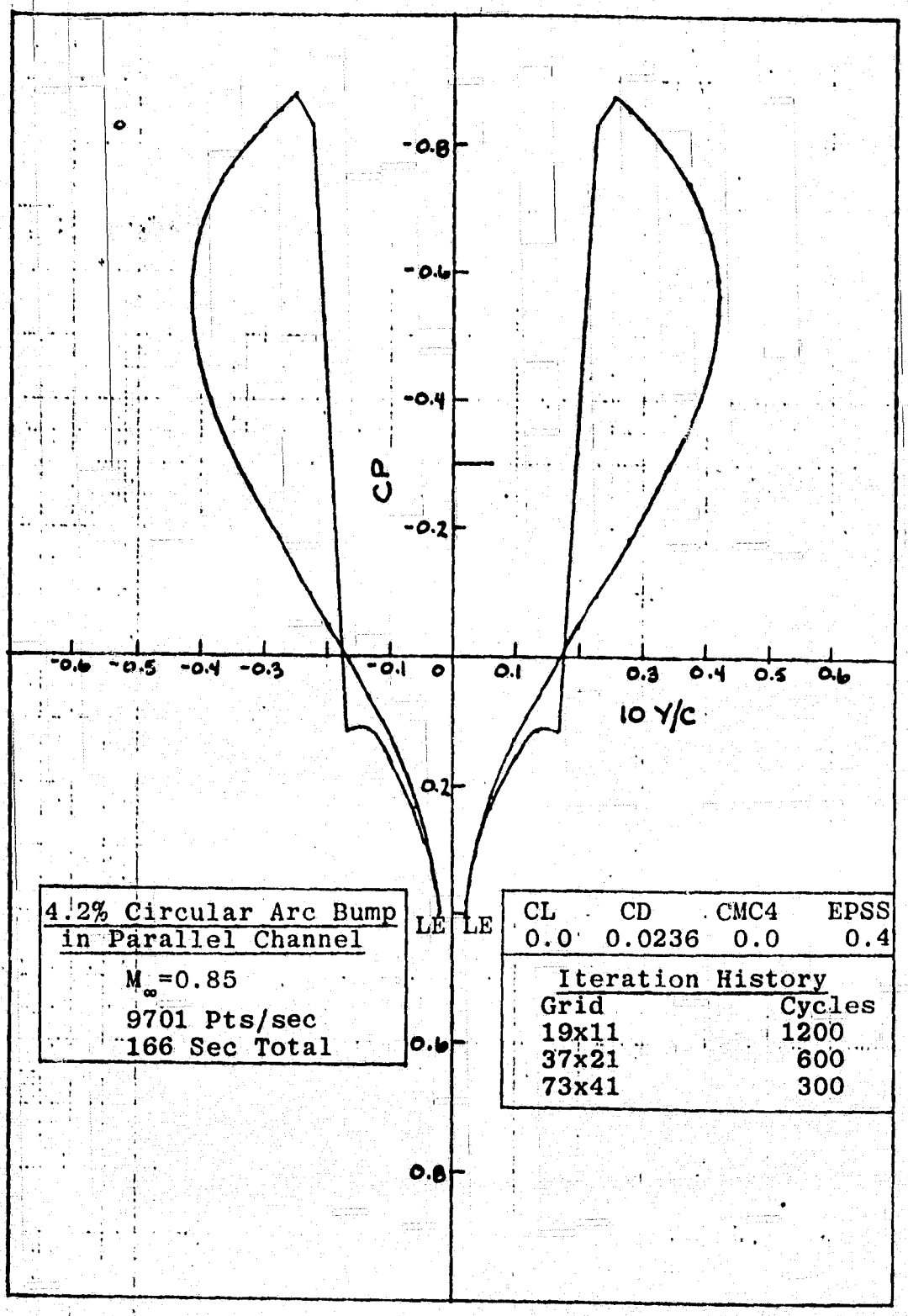

Figure 20a: Case B,"Bump" C_p Distribution versus Y/C, Floater Solution

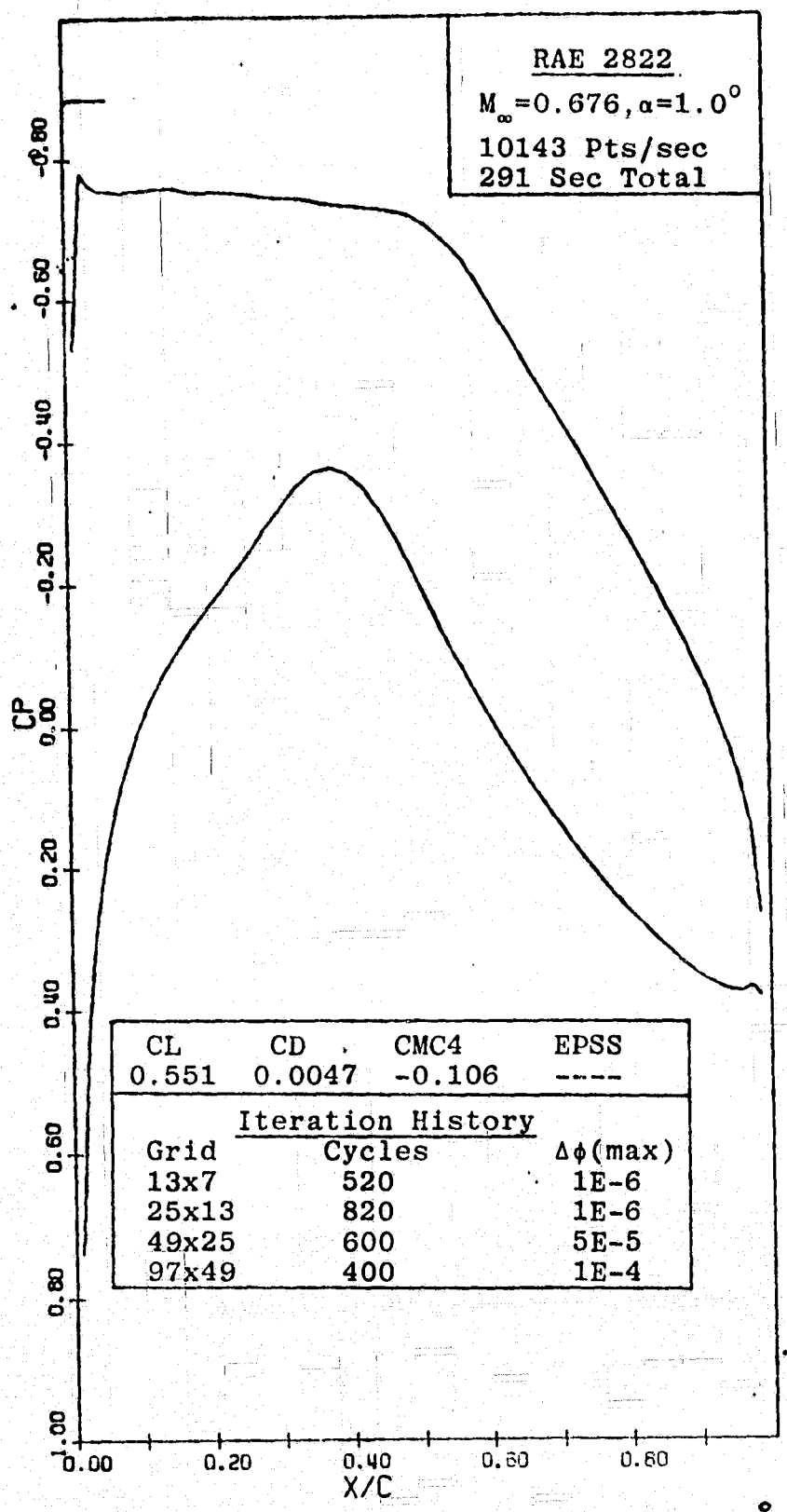

Figure 21: Case C-I, Airfoil C_p Distribution versus X/C

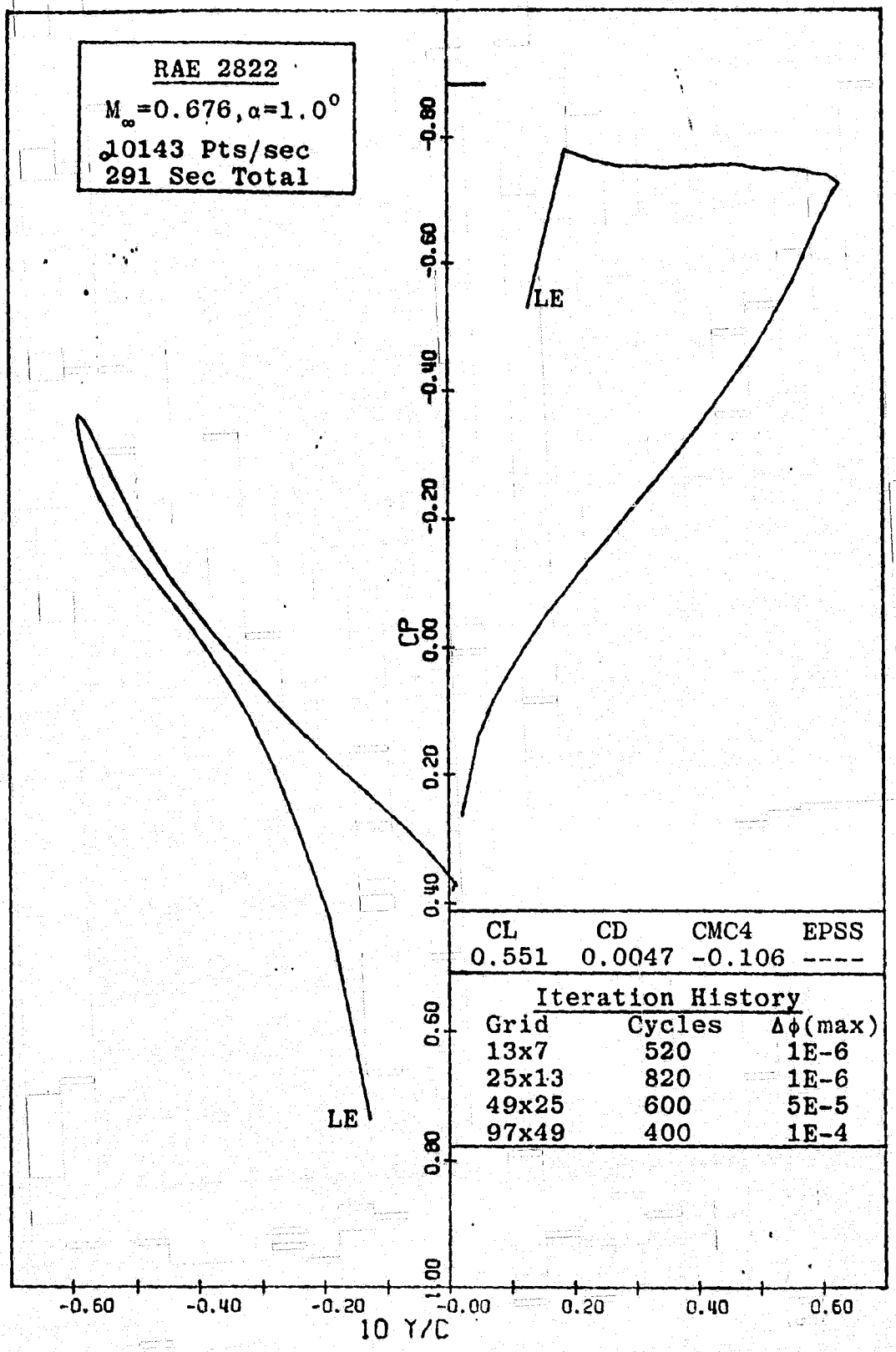

Figure 22: Case C-I, Airfoil C_p Distribution versus Y/C

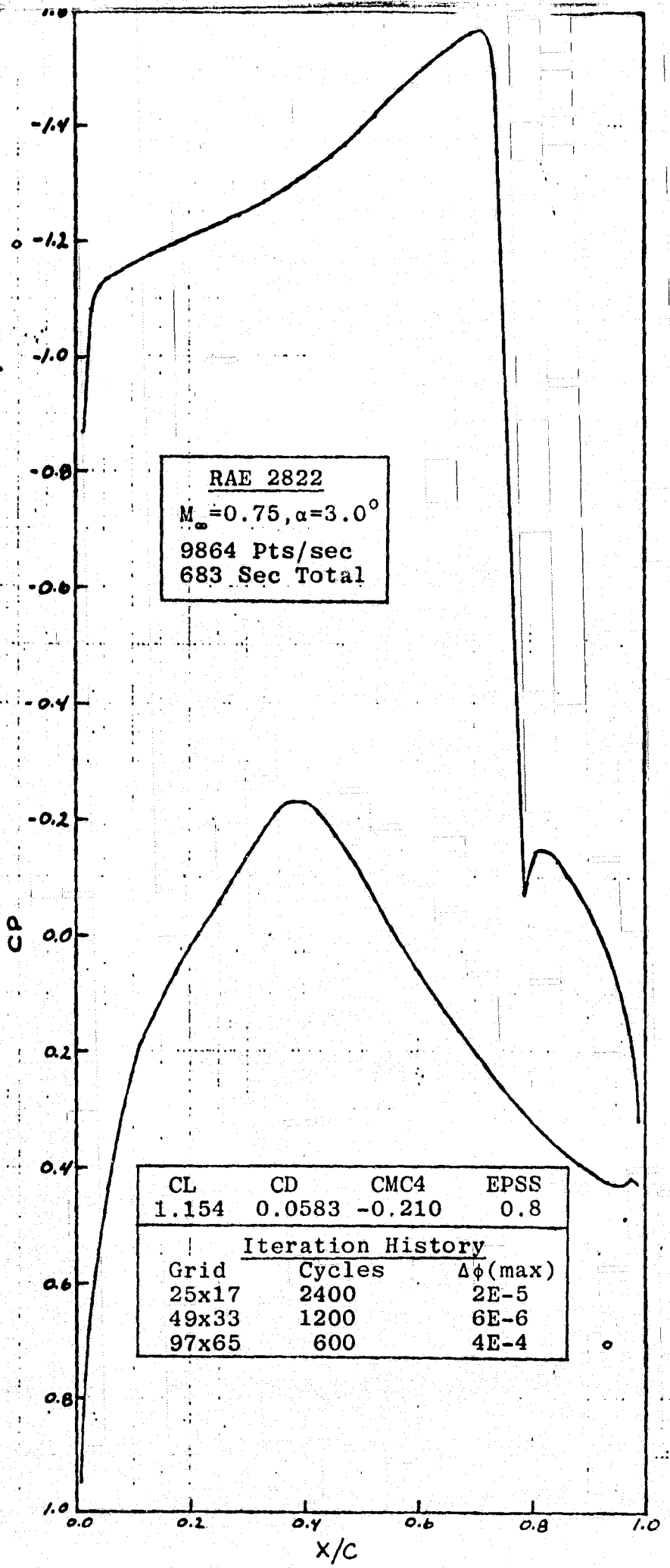

Figure 23: Case C-II, Airfoil C_p Distribution versus X/C

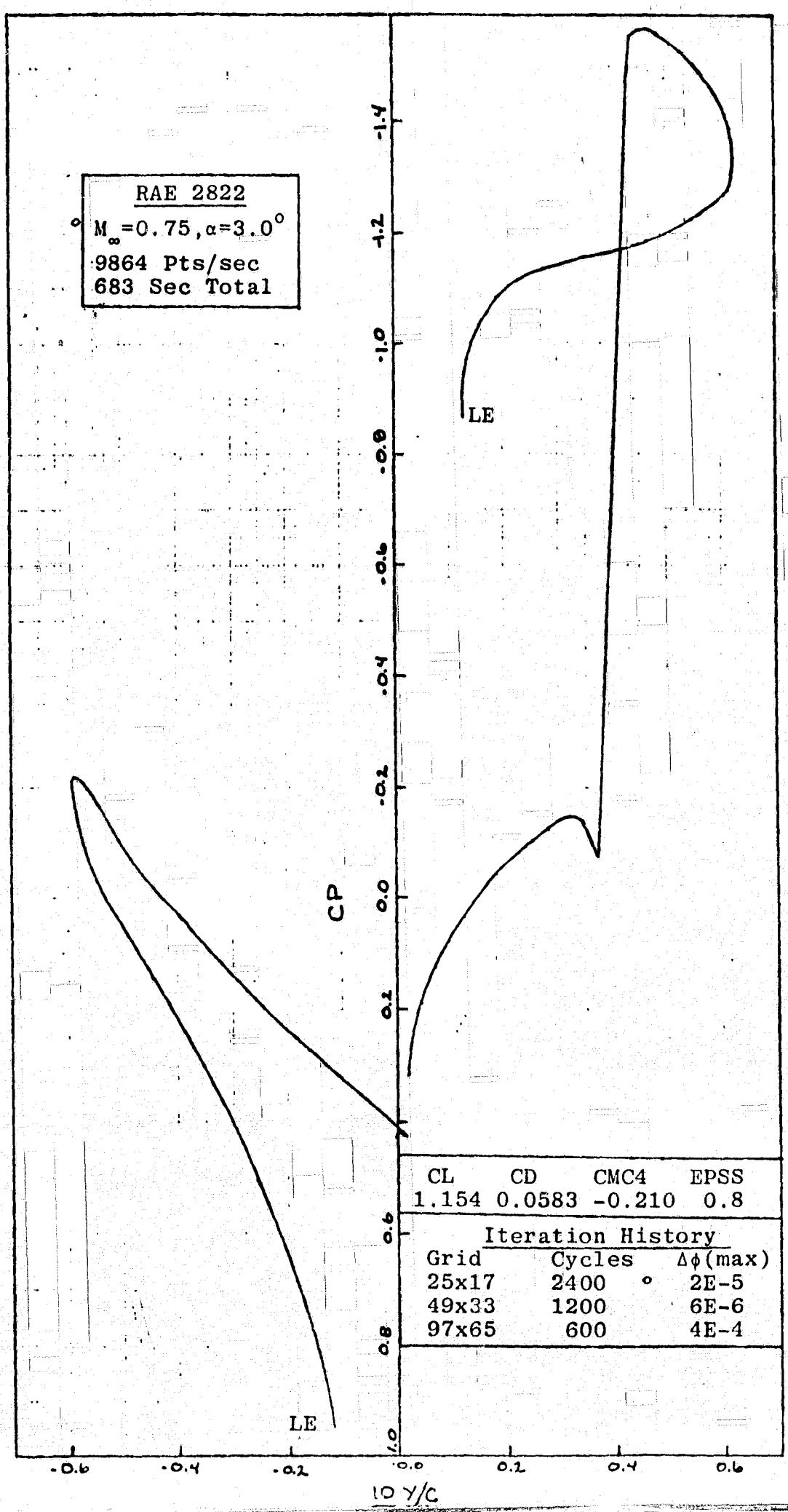

Figure 24: Case C-II, Airfoil C_p Distribution versus Y/C

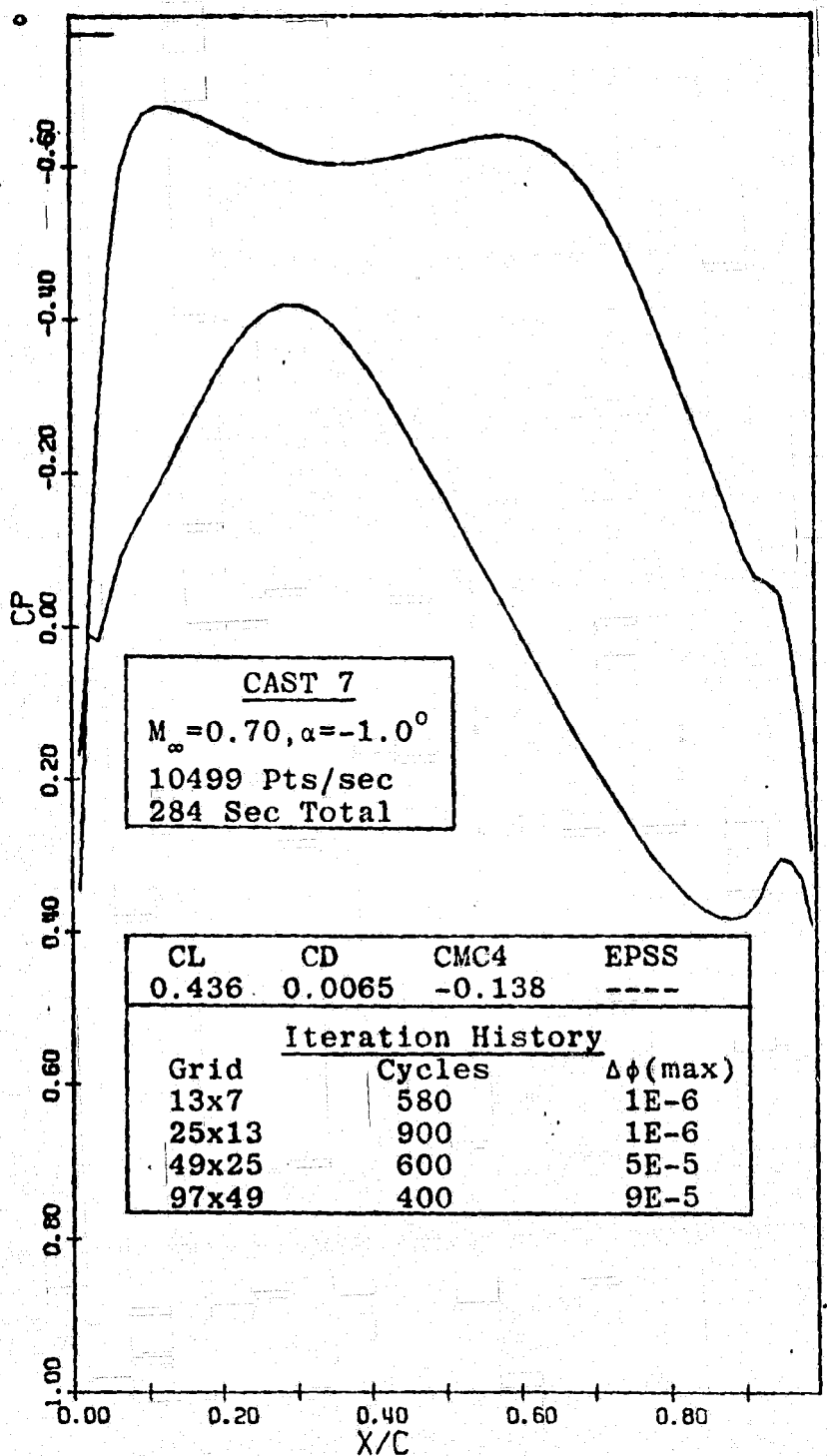

Figure 25: Case D-I, Airfoil C_p Distribution versus X/C

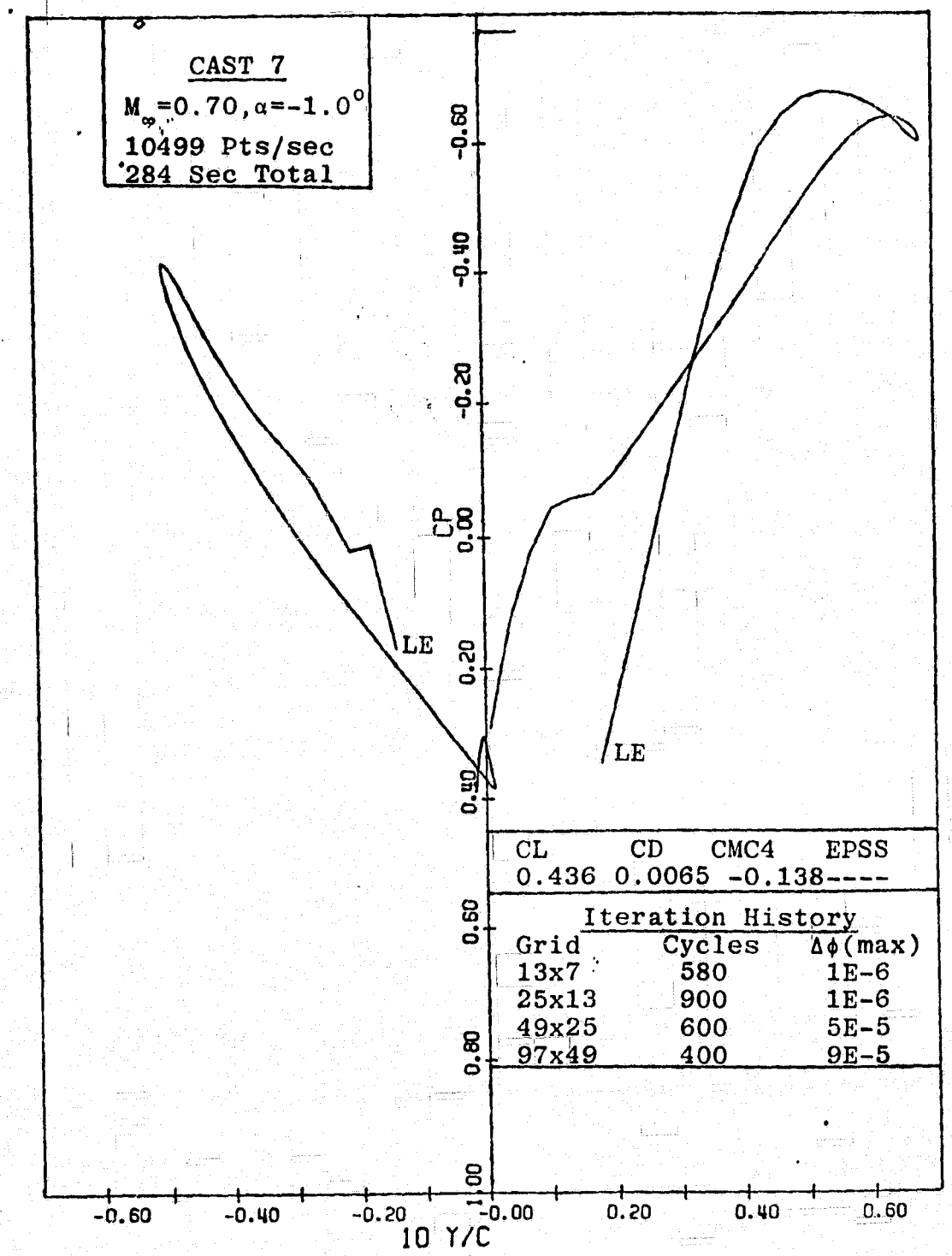

Figure 26: Case D-I, Airfoil C_p Distribution versus Y/C

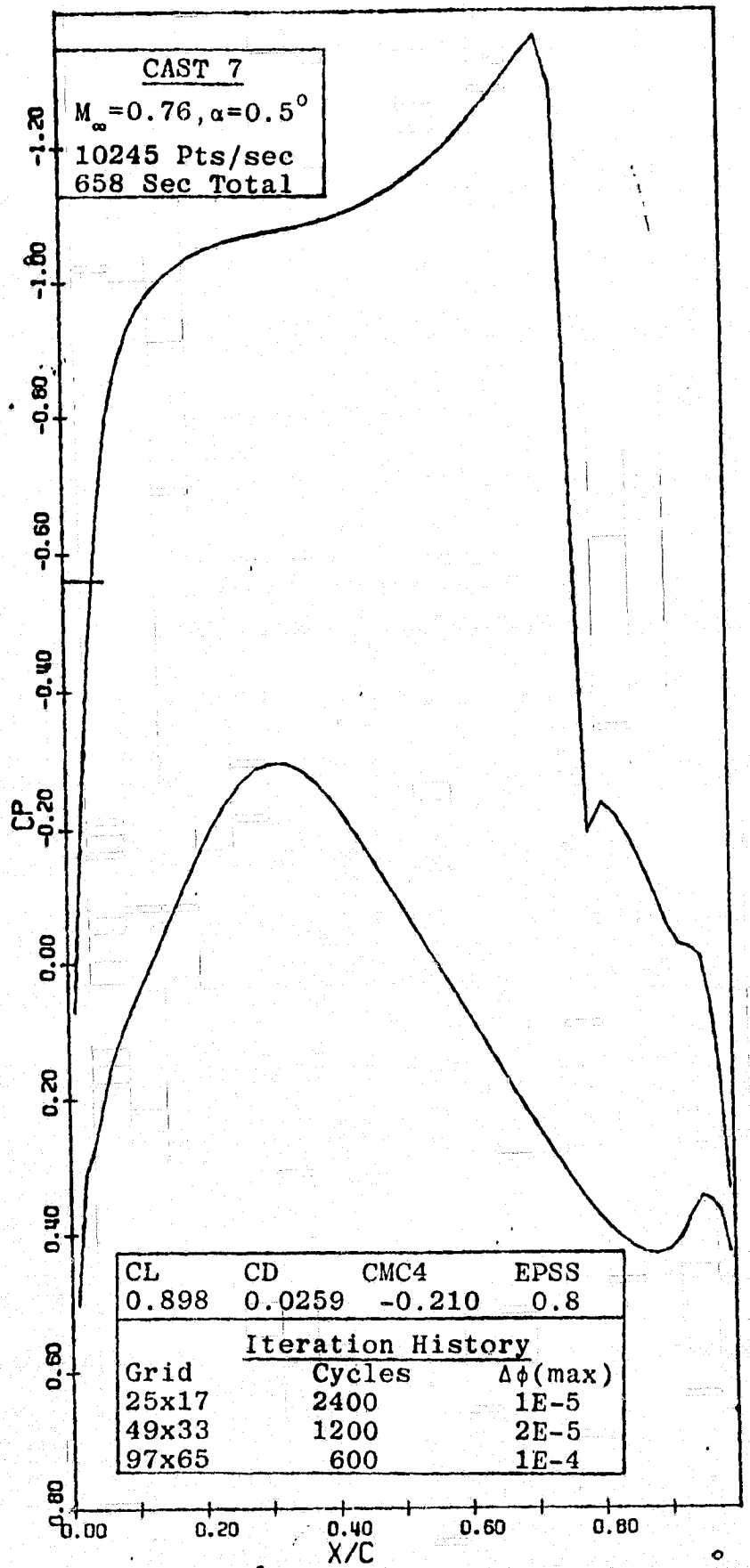

Figure 27: Case D-II, Airfoil C_p Distribution versus X/C

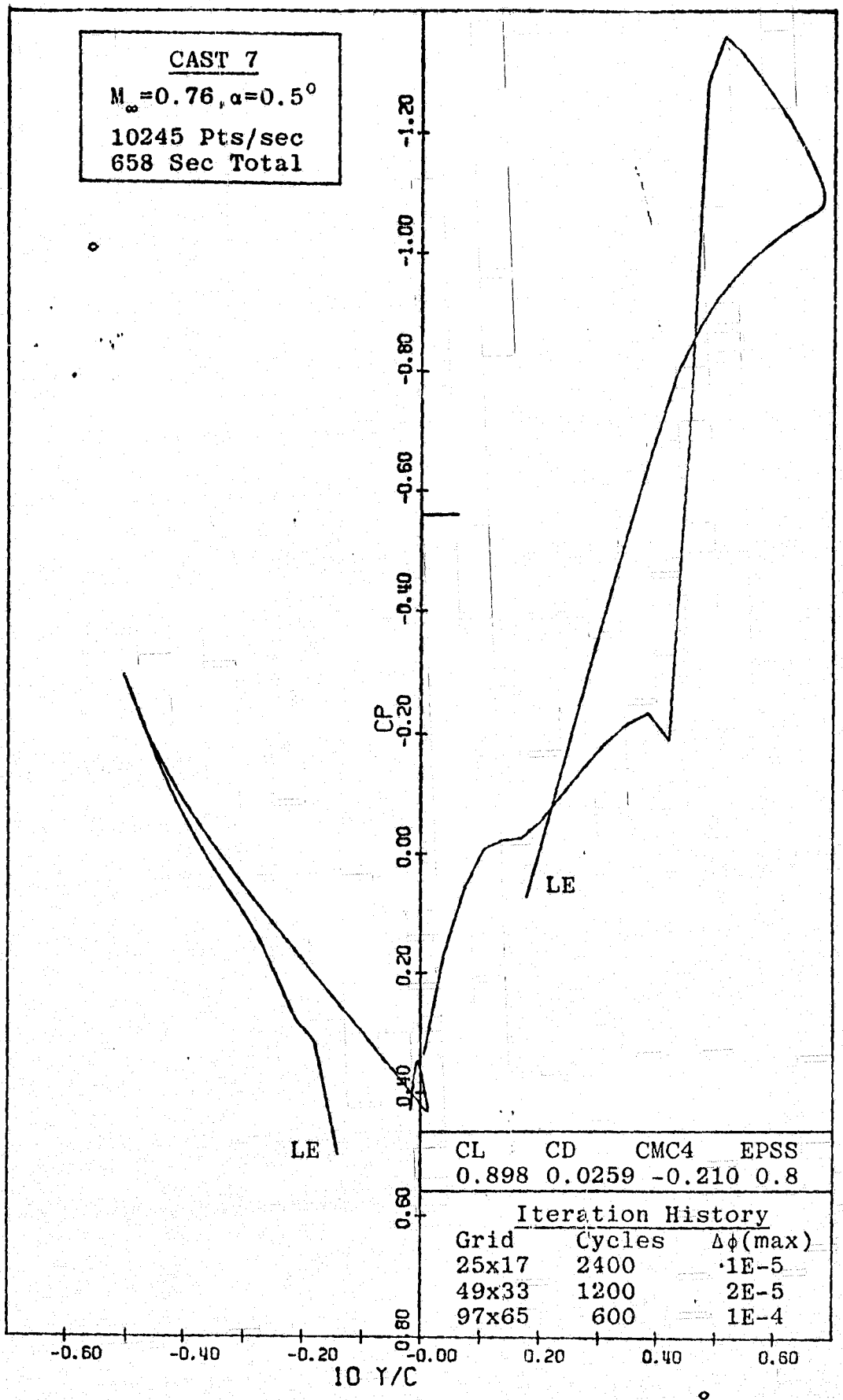

Figure 28: Case D-II, Airfoil C_p Distribution versus Y/C

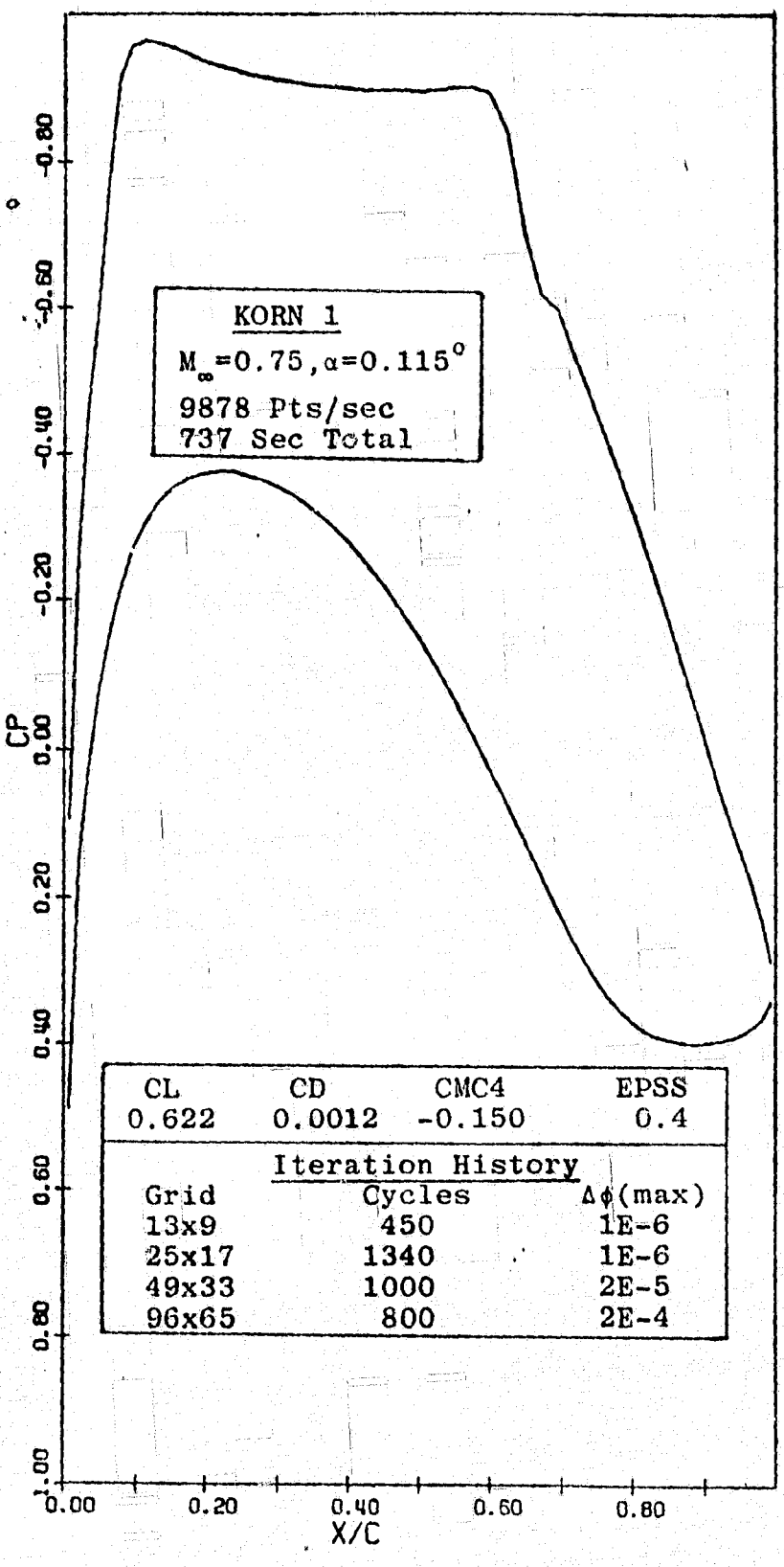

Figure 29: Case G-I, Airfoil C_p Distribution versus X/C

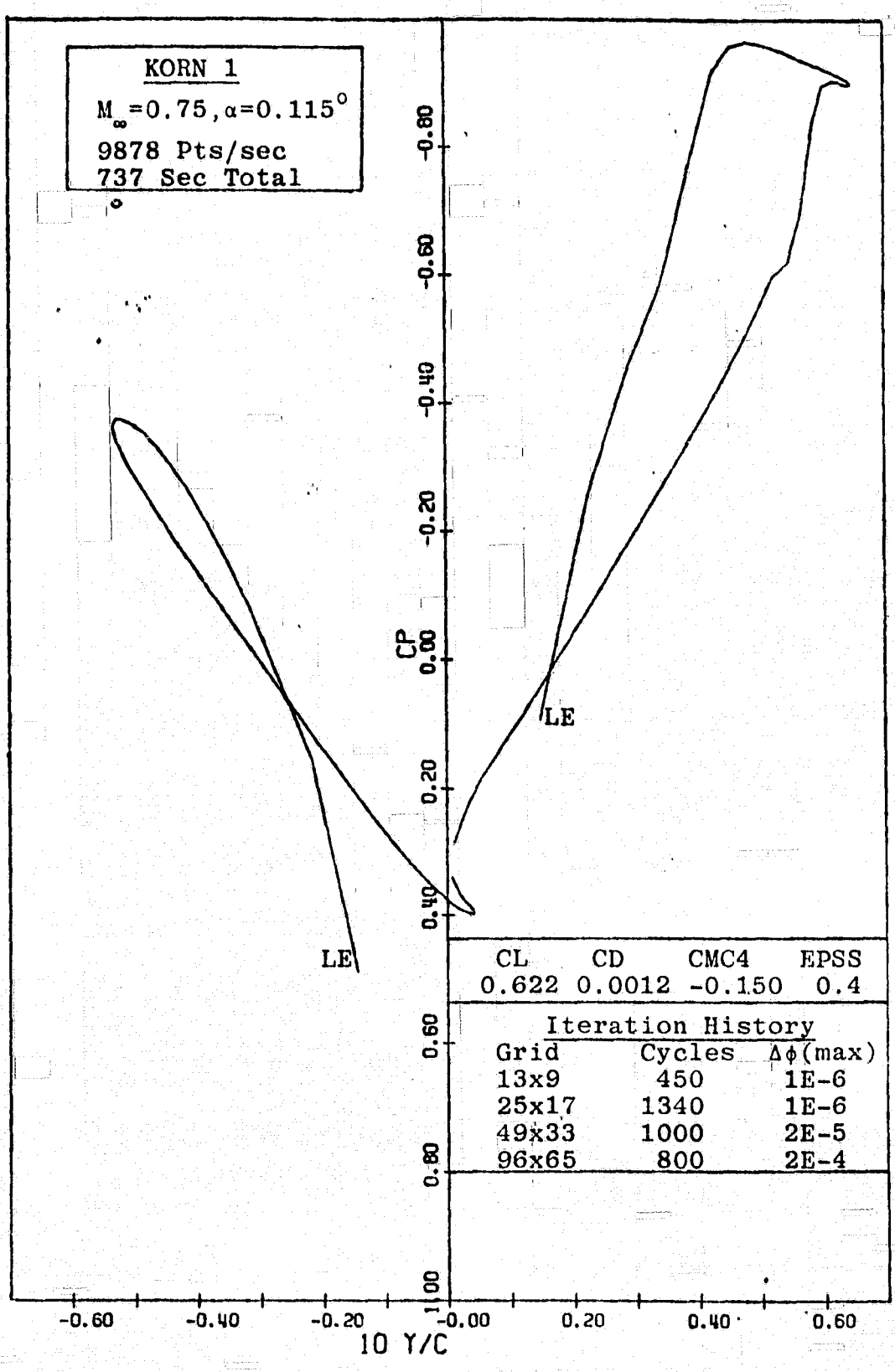

Figure 30: Case G-I, Airfoil C_p Distribution versus Y/C

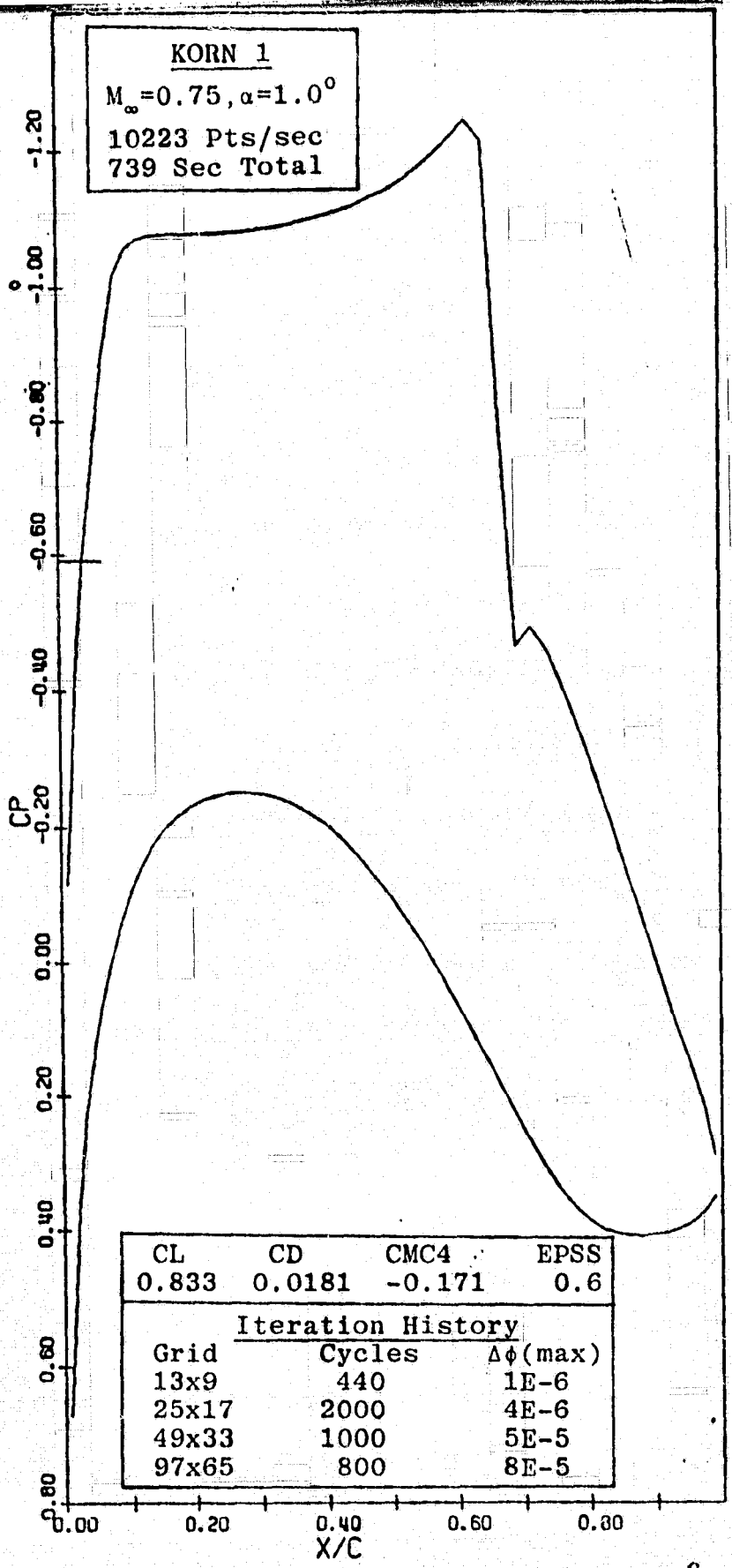

Figure 31: Case G-II, Airfoil C_p Distribution versus X/C

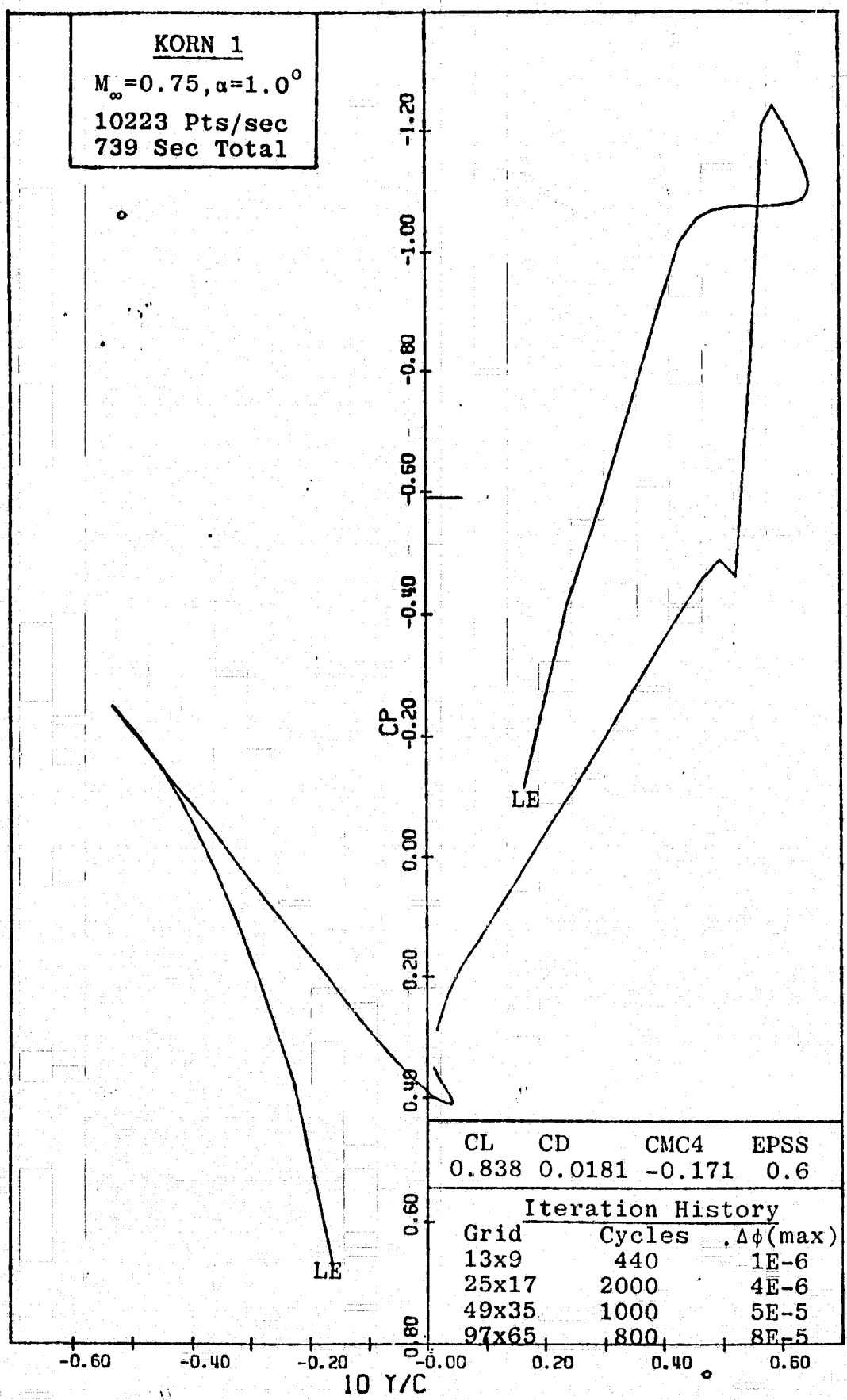

Figure 32: Case G-II, Airfoil C_p Distribution versus Y/C

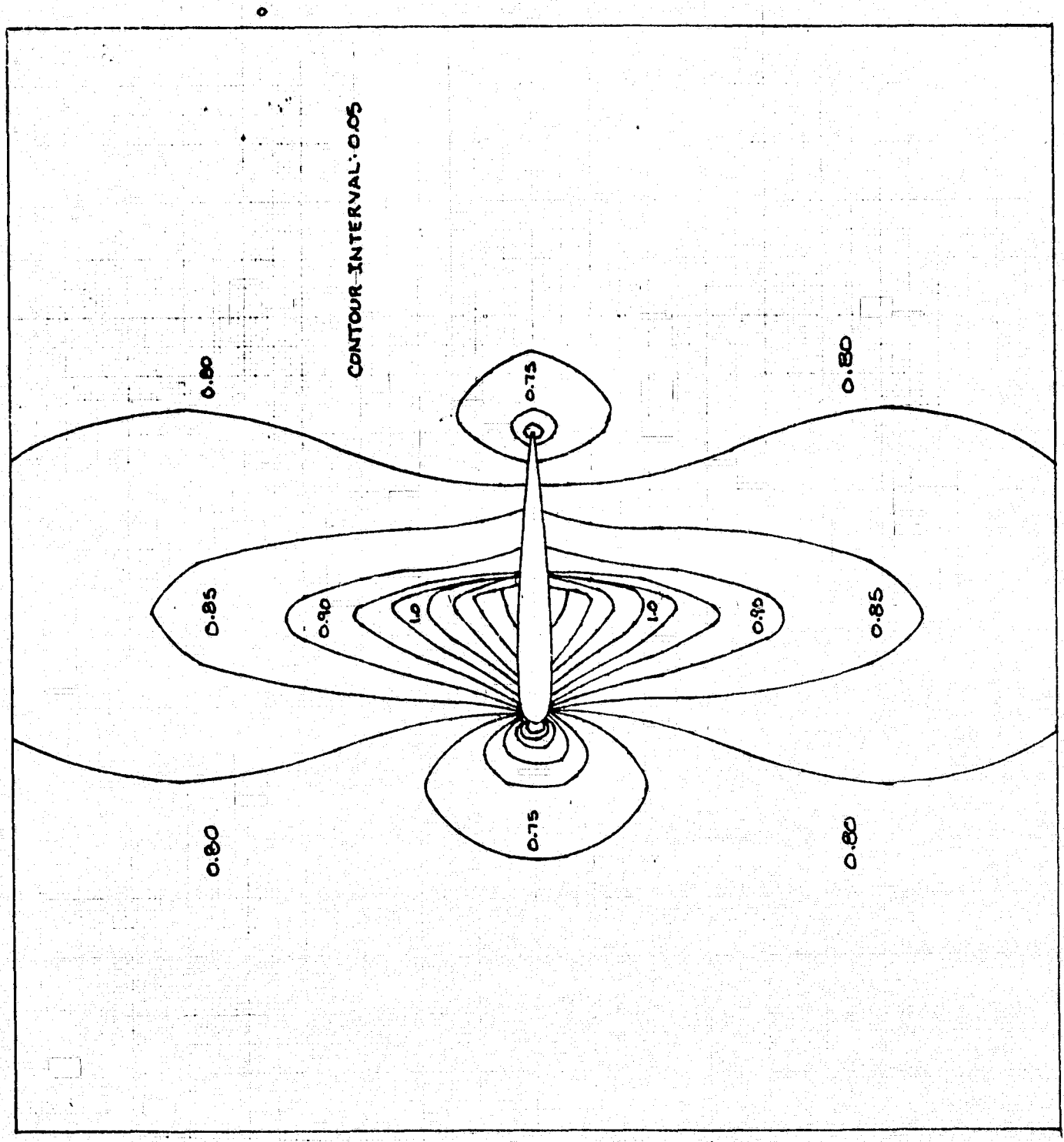

Figure 33 Mach Chart, NACA 0012, $M_\infty = 0.8$, $\alpha = 0°$.

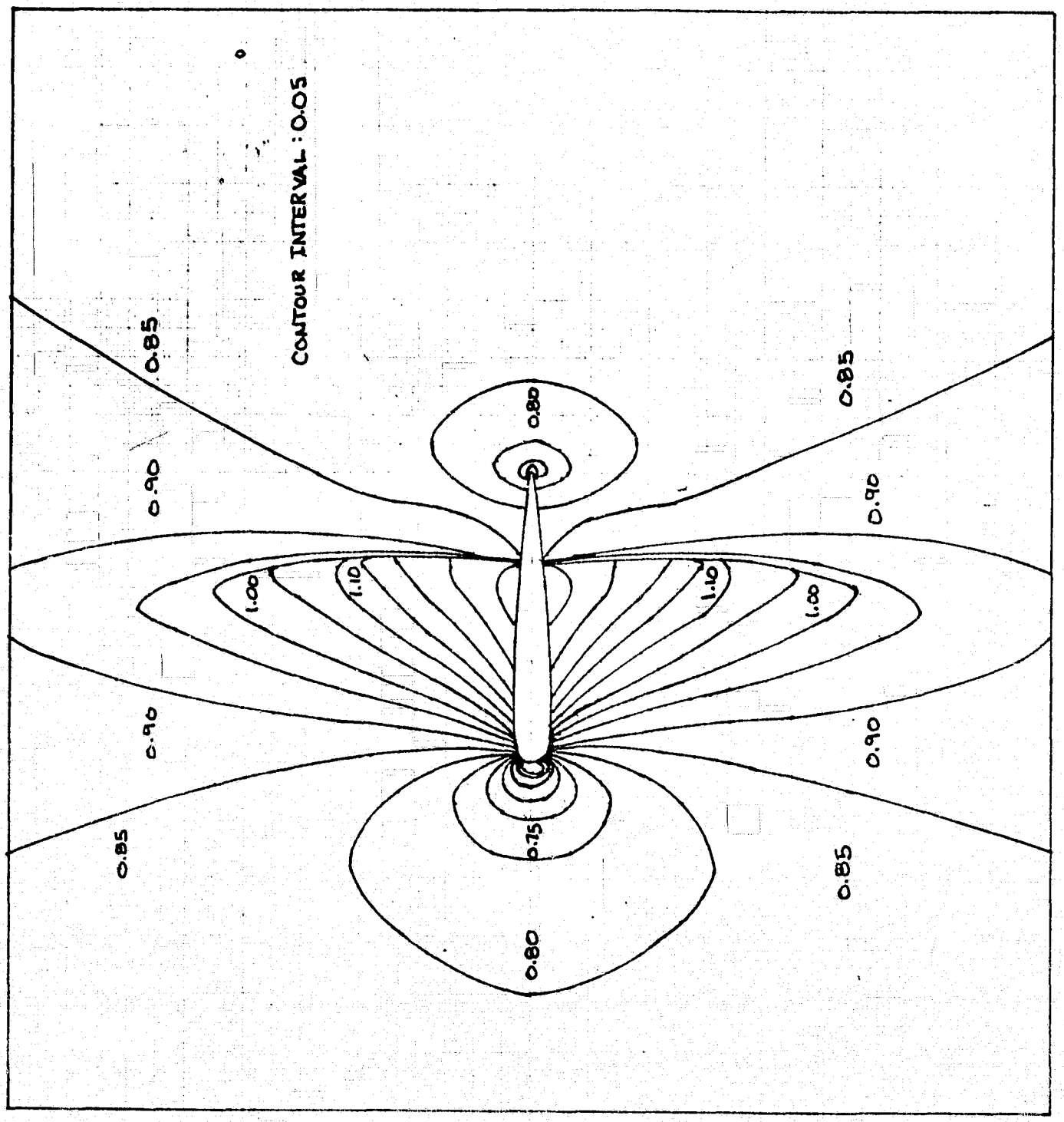

Figure 34 Mach Chart, NACA 0012, $M_\infty = 0.85$, $\alpha = 0°$.

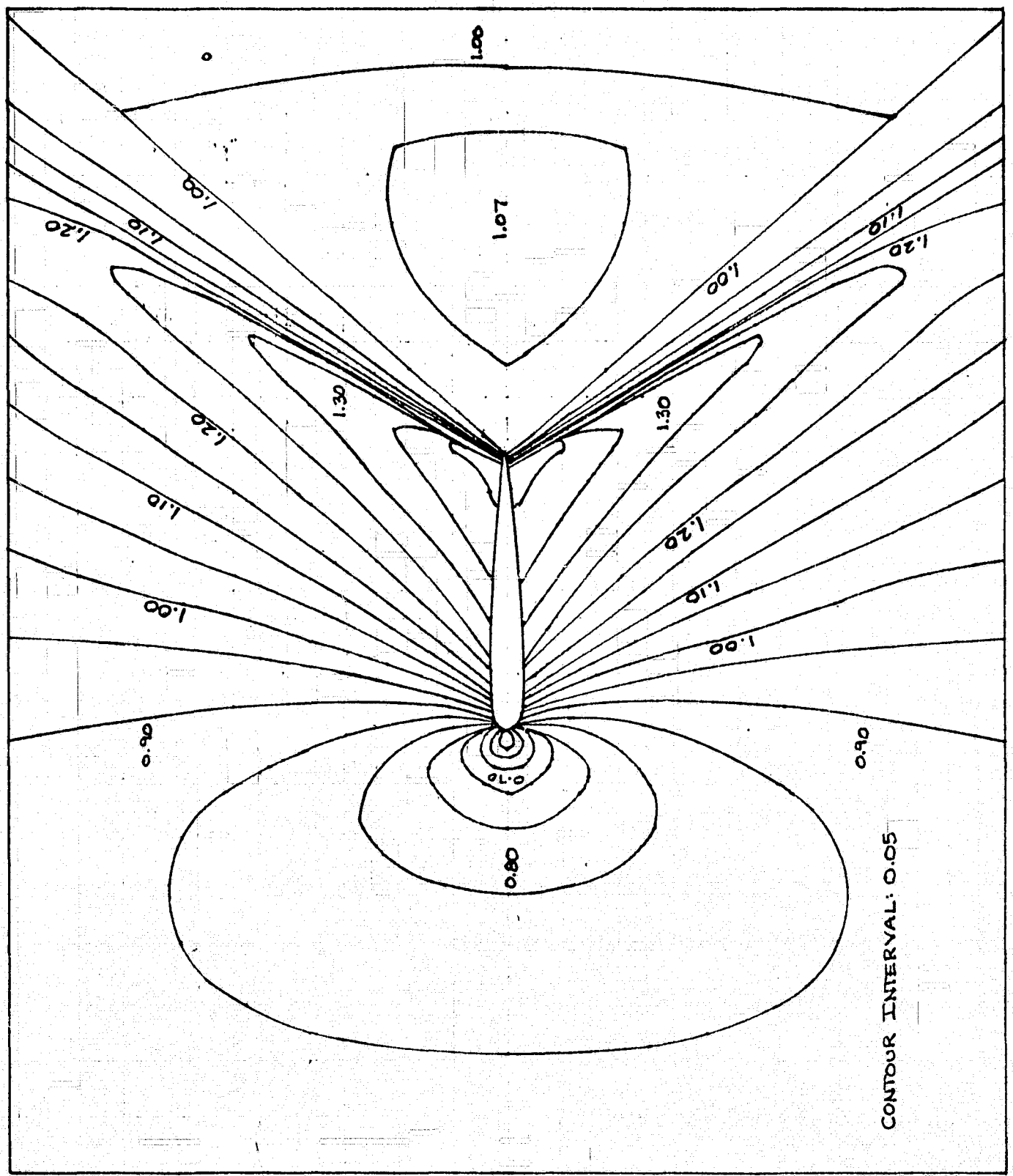

Figure 35 Mach Chart, NACA 0012, $M_\infty = 0.95$, $\alpha = 0°$.

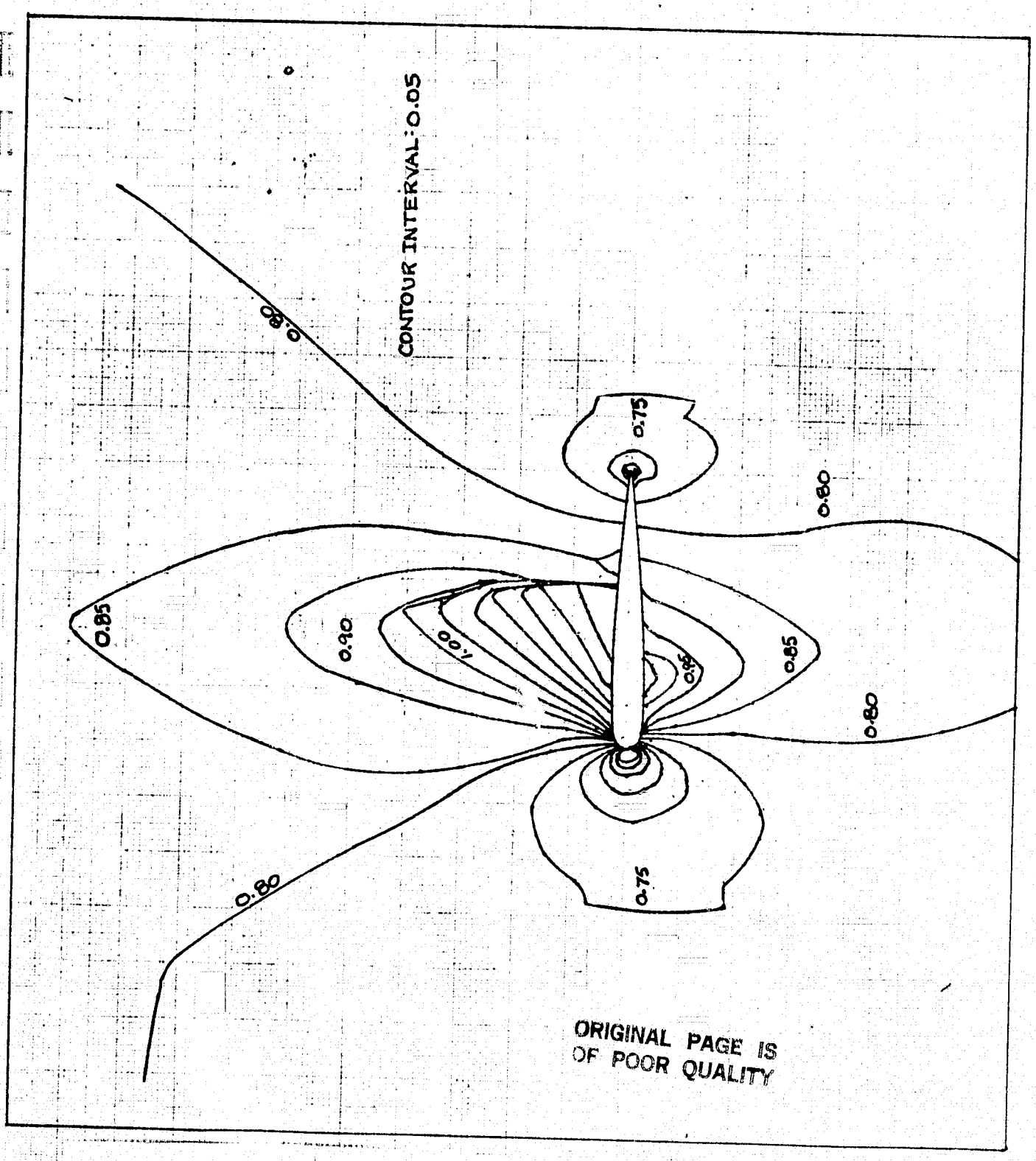

Figure 36 Mach Chart, NACA 0012, $M_\infty = 0.80$, $\alpha = 1.25°$.

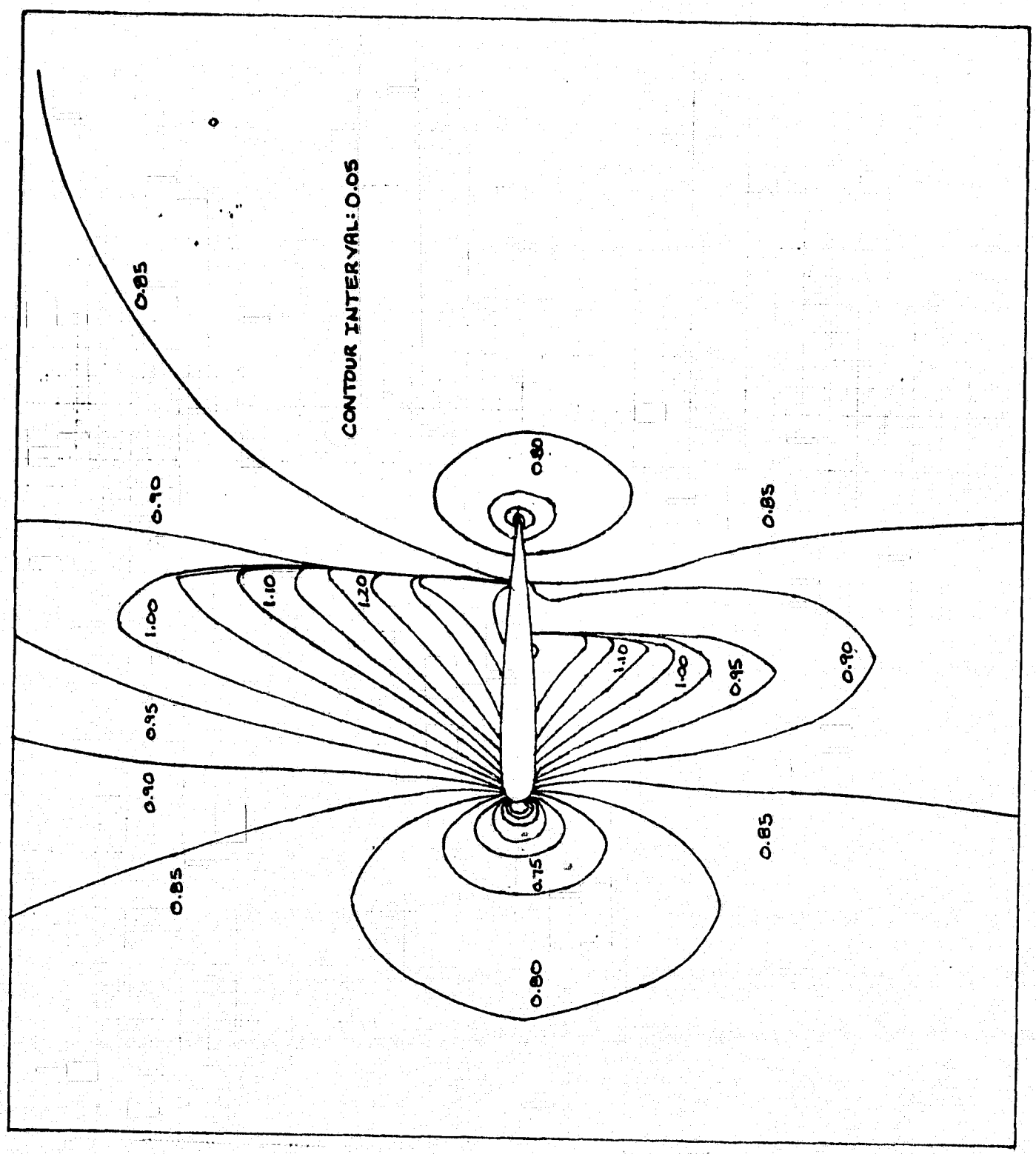

Figure 37 Mach Chart, NACA 0012, $M_\infty = 0.85$, $\alpha = 1°$.

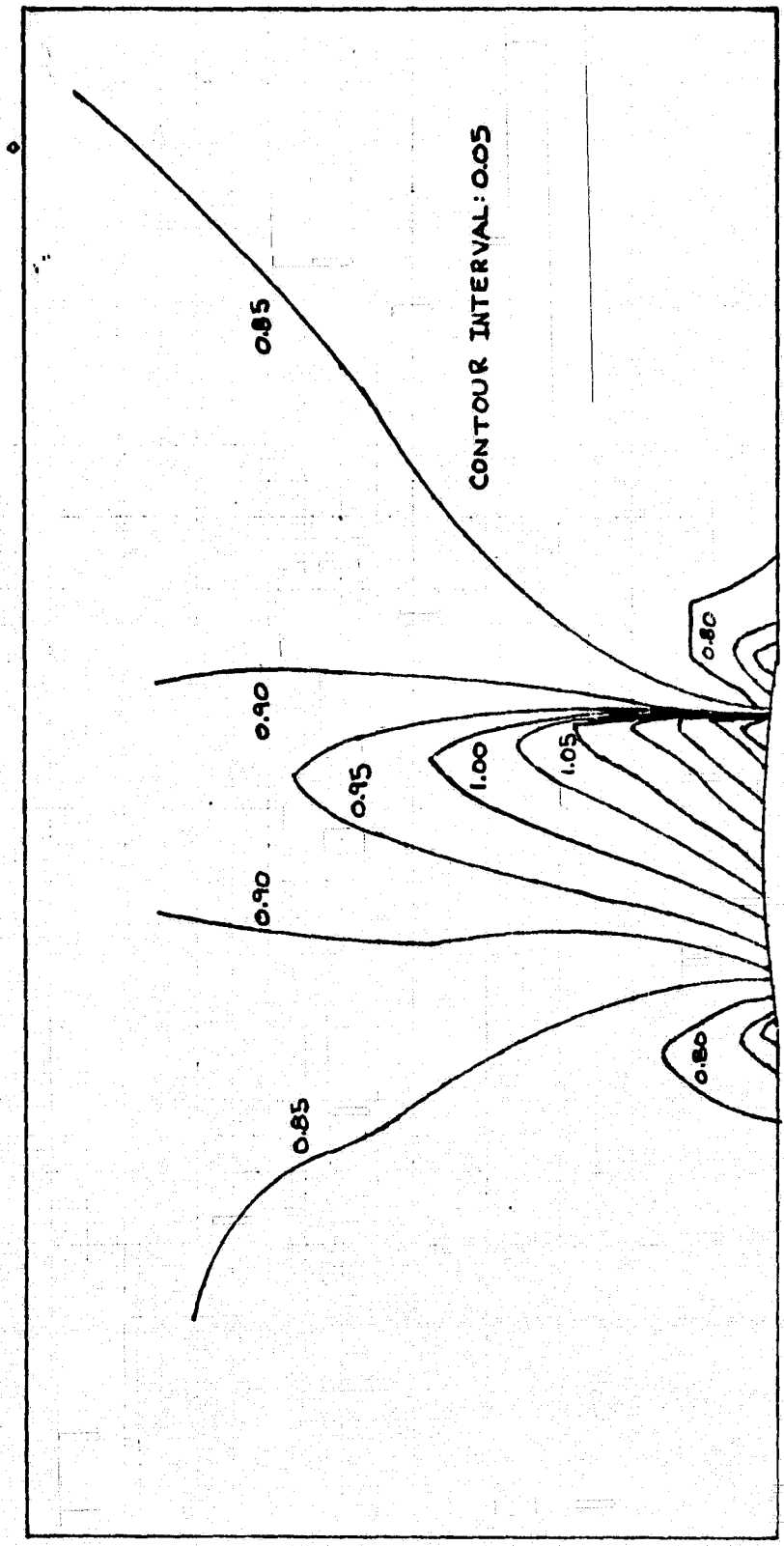

4.2% Bump M_∞ = 0.856

Figure 38 Mach Chart, 4.2% Bump in Channel, M_∞ = 0.856.

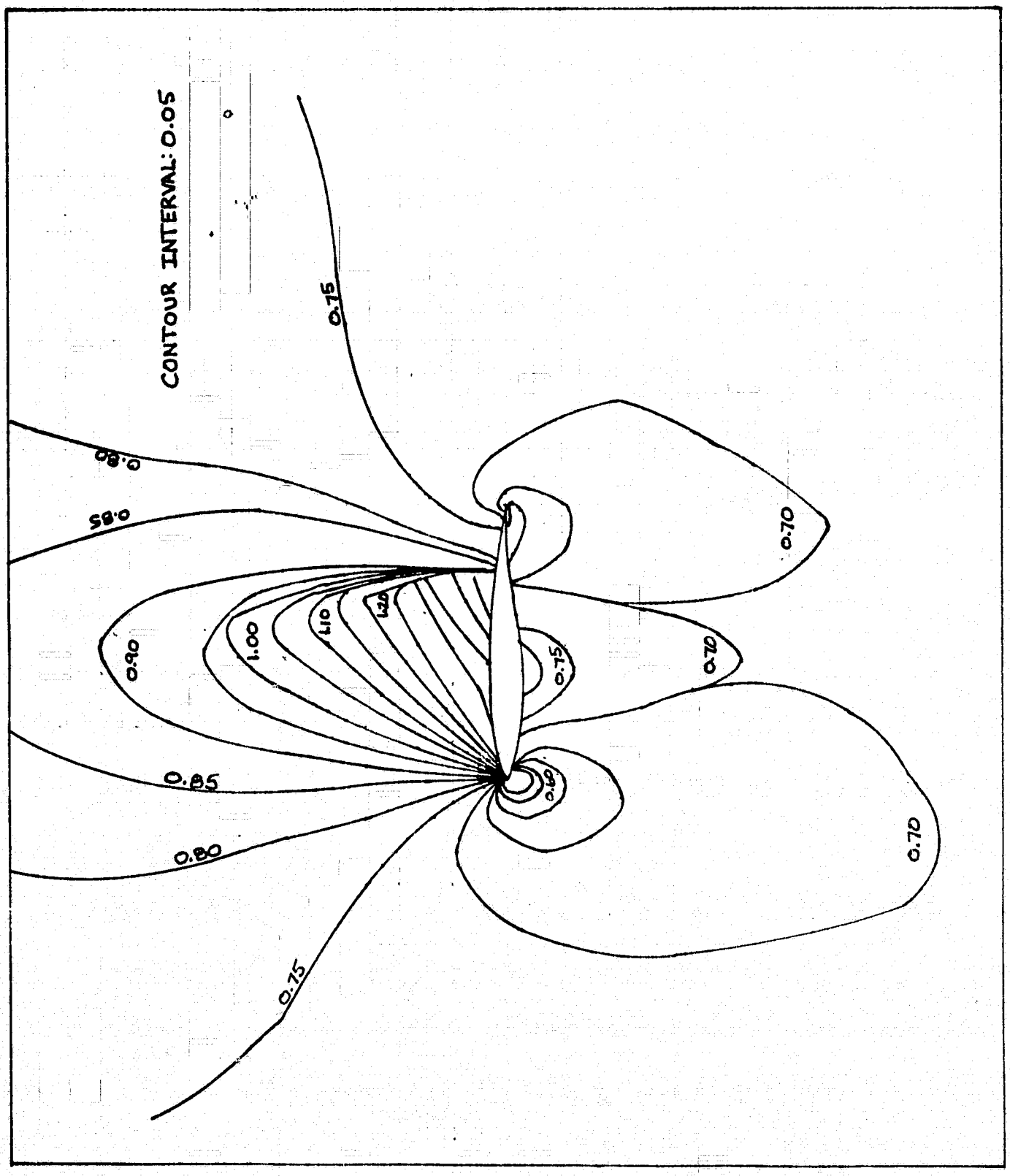

RAE 2822 $M_\infty = .75$ $\alpha = 3°$

Figure 39 Mach Chart, RAE 2822, $M_\infty = 0.75$, $\alpha = 3°$.

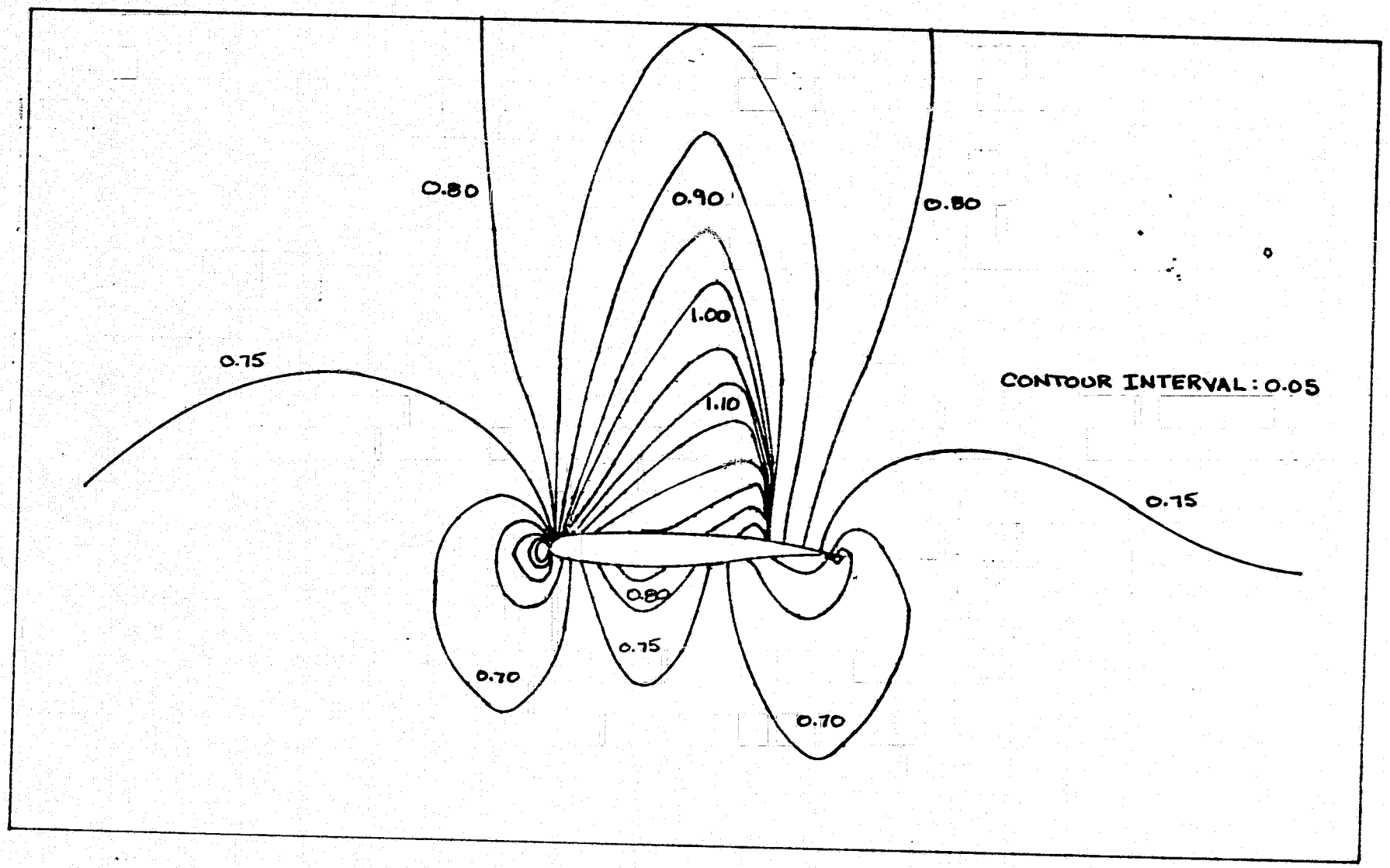

Figure 40 Mach Chart, CAST 7, $M_\infty = 0.76$, $\alpha = 0.5°$.

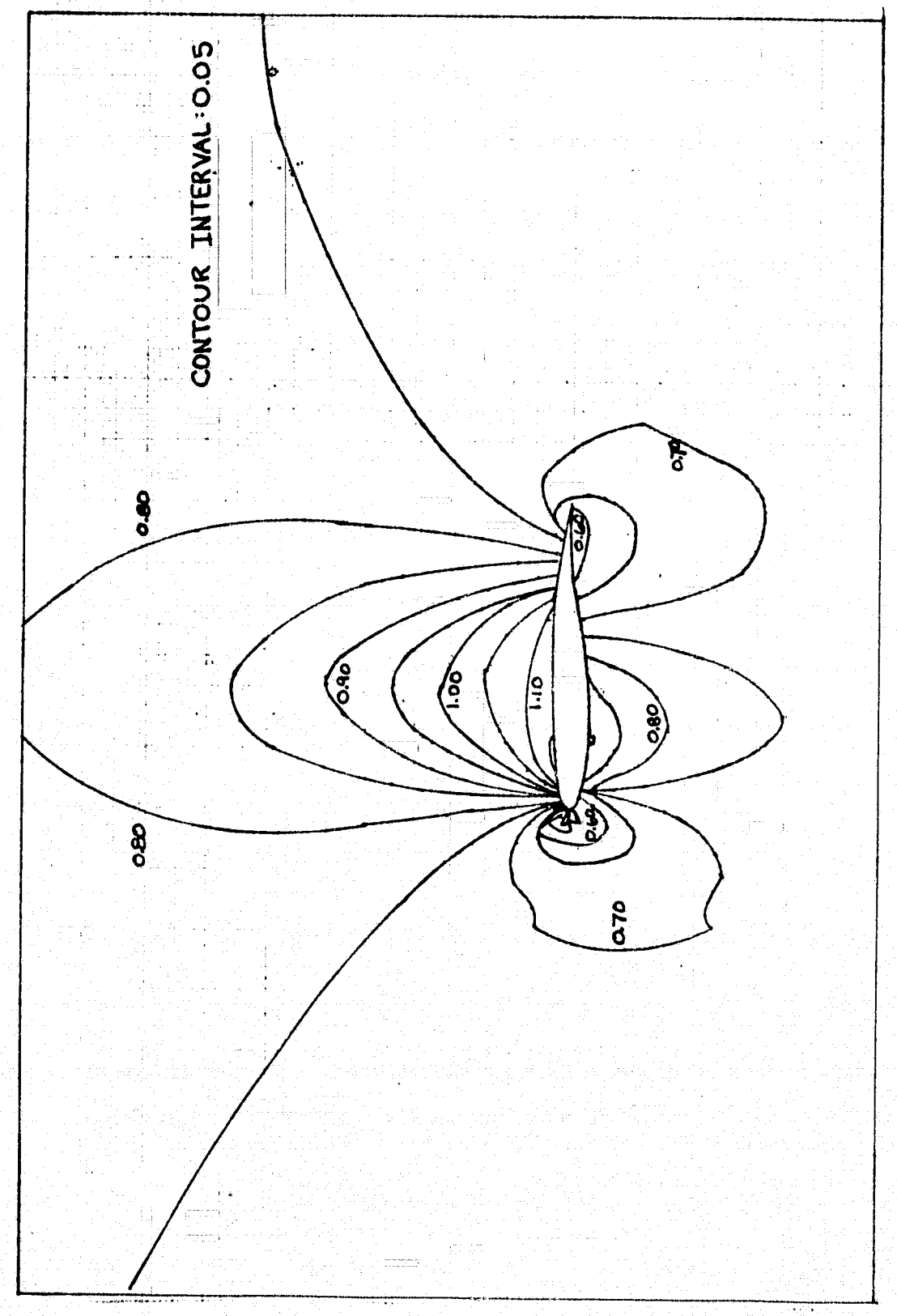

KORN 1
$M_\infty = .75$
$\alpha = .115°$

Figure 41 Mach Chart, KORN 1, $M_\infty = 0.75$, $\alpha = 0.115°$.

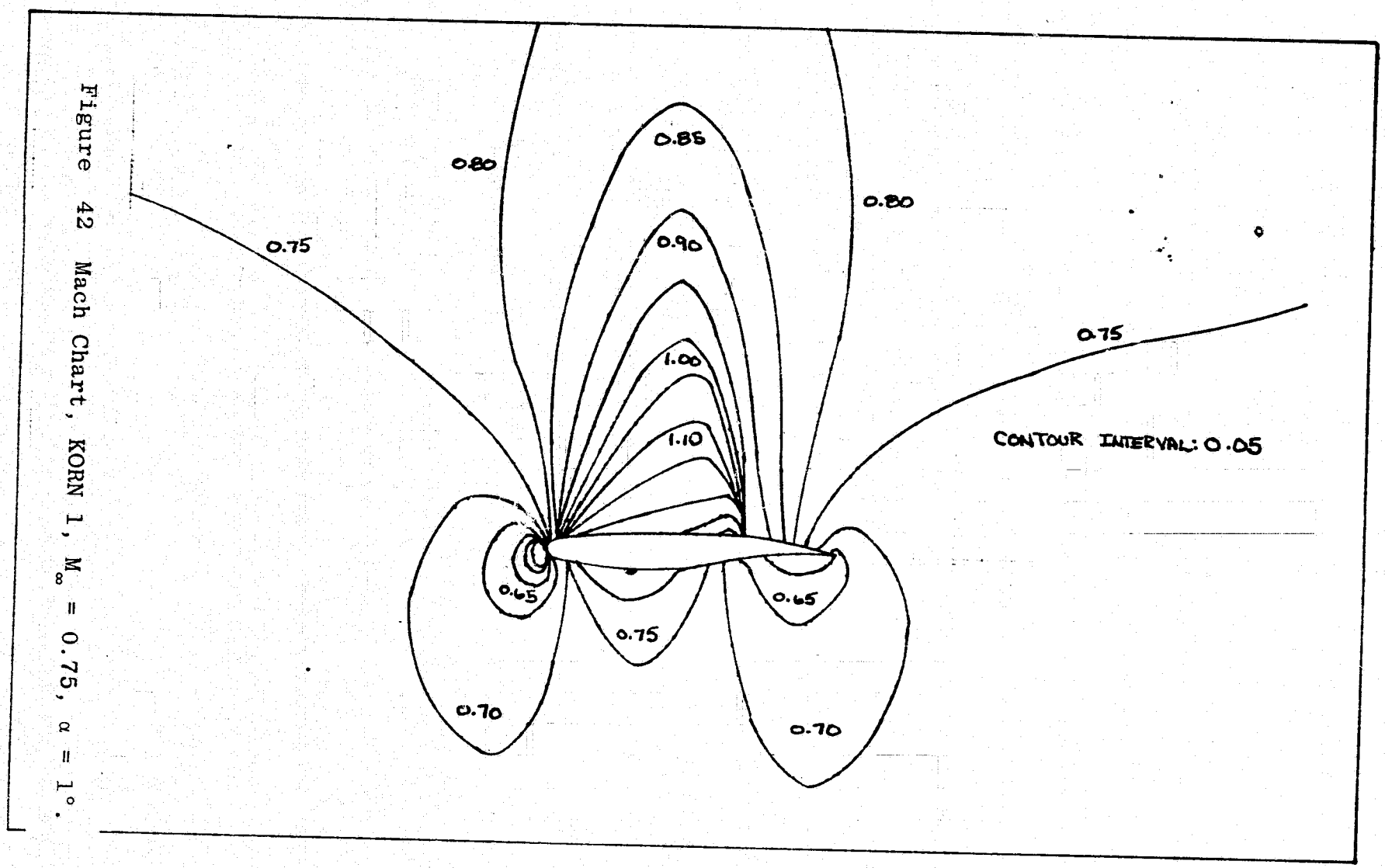

Figure 42 Mach Chart, KORN 1, $M_\infty = 0.75$, $\alpha = 1°$.

KORN 1
$M_\infty = 0.75$
$\alpha = 1°$